Chem Soc Rev

REVIEW ARTICLE

View Article Online
View Journal | View Issue

Cite this: *Chem. Soc. Rev.*, 2024, **53**, 1495

Crystalline porous organic salts

Guolong Xing, [abc] Daoling Peng [bd] and Teng Ben *[abc]

Crystalline porous organic salts (CPOSs), formed by the self-assembly of organic acids and organic bases through ionic bonding, possess definite structures and permanent porosity and have rapidly emerged as an important class of porous organic materials in recent years. By rationally designing and controlling tectons, acidity/basicity (pK_a), and topology, stable CPOSs with permanent porosity can be efficiently constructed. The characteristics of ionic bonds, charge-separated highly polar nano-confined channels, and permanent porosity endow CPOSs with unique physicochemical properties, offering extensive research opportunities for exploring their functionalities and application scenarios. In this review, we systematically summarize the latest progress in CPOS research, describe the synthetic strategies for synthesizing CPOSs, delineate their structural characteristics, and highlight the differences between CPOSs and hydrogen-bonded organic frameworks (HOFs). Furthermore, we provide an overview of the potential applications of CPOSs in areas such as negative linear compression (NLC), proton conduction, rapid transport of CO_2, selective and rapid transport of K^+ ions, atmospheric water harvesting (AWH), gas sorption, molecular rotors, fluorescence modulation, room-temperature phosphorescence (RTP) and catalysis. Finally, the challenges and future perspectives of CPOSs are presented.

Received 3rd October 2023

DOI: 10.1039/d3cs00855j

rsc.li/chem-soc-rev

[a] *Zhejiang Engineering Laboratory for Green Syntheses and Applications of Fluorine-Containing Specialty Chemicals, Institute of Advanced Fluorine-Containing Materials, Zhejiang Normal University, Jinhua, 321004, P. R. China. E-mail: tengben@zjnu.edu.cn*

[b] *Science and Technology Center for Quantum Biology, National Institute of Extremely-Weak Magnetic Field Infrastructure, Hangzhou 310000, P. R. China*

[c] *Key Laboratory of the Ministry of Education for Advanced Catalysis Materials, Institute of Physical Chemistry, Zhejiang Normal University, Jinhua, 321004, P. R. China*

[d] *Key Laboratory of Theoretical Chemistry of Environment, Ministry of Education, School of Environment, South China Normal University, Guangzhou 510006, P. R. China*

1. Introduction

Porous structures represent a significant structural motif in nature, endowing materials with extensive surface areas and internal channels that facilitate the adsorption, transport, and reaction of substances, thereby playing pivotal roles in life's evolution and evolutionary processes.[1,2] Inspired by the porous structures found in nature, scientists have successfully synthesized a variety of novel porous organic materials.[3] These materials mimic porous systems in nature and offer precise

Guolong Xing

Dr Guolong Xing received his BSc degree in chemistry from Jilin University (China) in 2012 and his PhD degree in polymer chemistry and physics from Jilin University under the supervision of Prof. Teng Ben in 2018. He then joined Prof. Long Chen's group as a lecturer at Tianjin University (China). In 2021, he moved to Zhejiang Normal University and joined Prof. Teng Ben's group. His current scientific interest focuses on the design and synthesis of crystalline porous organic materials.

Daoling Peng

Prof. Daoling Peng received his BSc and PhD degrees from Peking University (China) under the supervision of Prof. Wenjian Liu in 2000 and 2007, respectively. Then he worked with Prof. Kimihiko Hirao at Tokyo University and Prof. Markus Reiher at ETH Zurich as a postdoctoral fellow during 2007–2013. He joined South China Normal University as a professor of chemistry in 2013. His research interests are in the areas of density functional theory, computational materials design and relativistic quantum chemistry.

Table 1 Categories of porous organic materials

Building blocks	Chemical bond	Porous organic materials	
Organic building blocks	Covalent bond	HCPs, CMPs, PIMs, PAFs	Amorphous
		COFs	Crystalline
	Covalent bond and weak interaction	POCs	Crystalline
	Hydrogen bond	HOFs	Crystalline
	Ionic bond	CPOSs	Crystalline

control over their structure and properties through sophisticated design and synthesis, thus imparting them with specific physicochemical properties and functionalities.[4]

The past few decades have witnessed the rapid development of porous organic materials. This diverse plethora of porous organic materials has shown tremendous potential in catalysis, adsorption, separation, energy storage and conversion, ecological environments, and other fields, which clearly demonstrates that porous organic materials are exceedingly promising materials with a bright and prosperous future ahead.[3] Porous organic materials are constructed by connecting organic building blocks through different types of chemical bonds, allowing for their classification based on the nature of the bonds (Table 1). For instance, covalent bonds can give rise to a plethora of porous organic materials such as hypercrosslinked polymers (HCPs),[5–7] conjugated microporous polymers (CMPs),[8–10] polymers of intrinsic microporosity (PIMs),[11–13] porous aromatic frameworks (PAFs),[14–16] and covalent organic frameworks (COFs).[17–19] Those formed through the synergy of covalent bonds and weak intermolecular interactions are consequently coined porous organic cages (POCs).[20–22] The utilization of hydrogen bonds yields porous organic materials known as HOFs.[23–25] In contrast, ionic bonds facilitate the formation of porous organic materials termed CPOSs.[26–38] Depending on their long-range structural order, these materials can further be categorized as amorphous or crystalline porous organic materials.

Teng Ben

Prof. Teng Ben obtained BSc and PhD degrees from Jilin University (China) in 1997 and 2002, respectively, and started teaching in the Department of Chemistry, Jilin University. He then worked as a postdoc fellow (Japan Society for the Promotion of Science (JSPS), 2005–2007; Japan Science and Technology Agency (JST), 2007–2008) at Nagoya University. In 2010, he was promoted to full professor at the College of Chemistry, Jilin University. Since 2021, he has worked at Zhejiang Normal University as a Distinguished Professor. His research interests include the fundamental understanding of host–guest interactions in nanoporous materials, gas storage, and separation using porous organic frameworks.

Amorphous porous organic materials primarily encompass HCPs, PAFs, CMPs, and PIMs. These materials are formed through the connection of organic building blocks *via* covalent bonds, exhibiting a pronounced porosity and exceptional performance for catalysis, gas storage and separation, energy storage and conversion, and sensing, among other applications. However, the inherent structural disorder poses limitations to elucidating their structure–function relationships, thereby impeding research progress on amorphous porous organic materials to a certain extent.

Crystalline porous organic materials primarily encompass COFs, HOFs, POCs, and CPOSs. These materials are constructed through the assembly of organic building blocks *via* distinct chemical bonds, showcasing remarkable features such as architecturally tailored structures and high porosity. Additionally, the definiteness of the structure also offers convenience in the explication of structure–function relationships.

COFs are a class of crystalline porous organic materials with tailored structures formed by linking organic building blocks through covalent bonds. Since Yaghi's[39] pioneering report in 2005, COFs have experienced rapid advancements due to their outstanding stability, high surface area, and designable structure. By incorporating concepts from reticular chemistry, a plethora of two-dimensional (2D) and three-dimensional (3D) COFs, possessing diverse linkages, have been synthesized, significantly expanding the structural diversity and functionality of COFs.[40,41]

POCs were first reported by Cooper[42] in 2009. Unlike COFs, HOFs, and other crystalline porous materials, the connection of organic building blocks through covalent bonds initiates the formation of organic cages, which are further assembled into ordered porous structures through weak intermolecular interactions, giving rise to POCs.[43,44] The pores of POCs comprise the cavities within the cages and interconnecting channels formed upon the cage stacking. Consequently, POCs possess a distinctive advantage in solubility compared with traditional metal–organic frameworks (MOFs) and COFs, allowing for convenient solution processing.

HOFs represent a class of crystalline porous organic materials with open frameworks self-assembled from organic building blocks through hydrogen bonding. The reversible and flexible nature of hydrogen bonds imparts HOFs with exceptional attributes, including high crystallinity, solution processability, facile healing, and purification. These distinctive features have rendered HOFs with immense potential for applications in vital fields such as gas storage and separation, molecular recognition, optoelectronic materials, chemical sensing, and catalysis.[23] The concept of HOFs was first proposed by Chen[45] in 2011, and over

the past decade, the field has undergone tremendous advancement in terms of both diversity and functionality. HOFs have developed into a relatively large and mature field with broad prospects for further advancement.

Herein, we introduce a unique and innovative class of crystalline porous organic materials called CPOSs. CPOSs have emerged as a burgeoning type of functional crystalline porous organic materials in recent years. Unlike the porous organic materials constructed from organic building blocks through covalent bonding, hydrogen bonding, and weak interactions mentioned above, CPOSs are assembled through ionic bonding between organic acids and organic bases, resulting in a regular structure with permanent porosity.[29] The highly polar nano-confined channels present in CPOS structures are reminiscent of inorganic porous materials known as zeolites. Zeolites[46–48] have unique polar pore structures and exceptional stability, and have already found commercial success as adsorbents and catalysts, and are extensively employed in crucial chemical and chemical engineering fields such as heterogeneous catalysis and the petrochemical industry, profoundly influencing the development of modern society. CPOSs, as a class of organic porous materials highly analogous to zeolites, can be referred to as ''organic zeolites'', and they show promising potential to achieve commercialization in the future similar to their inorganic counterparts.

Ionic bonding serves as a significantly pivotal interaction in the construction of CPOSs. However, despite its significance as a fundamental chemical bond, the direct utilization of ionic bonding for constructing porous organic materials has long remained a realm of unexplored research. In the early stages, Ward *et al.* conducted a significant amount of pioneering work[49–54] in the realm of constructing networks based on ionic bonding. They adeptly employed organic acids and bases to fabricate organic salt networks, deftly utilizing various organic sulfonic acids and guanidine to create an array of intricate patterns. This inventive approach enabled the successful synthesis of a series of network structures encapsulating guest molecules. Furthermore, White *et al.* employed ionic bonding to synthesize numerous organic salt networks[55–61] using organic carboxylic acids and amidines. Regrettably, these networks experienced structural collapse upon removing the guest molecules, thus lacking permanent porosity. Additionally, Tohnai *et al.* employed organic sulfonic acids and organic amines to successfully construct stable supramolecular clusters[62] through ionic bonding, and construct many salts[63–68] based on the supramolecular clusters. These early investigations significantly advanced the development and evolution of CPOSs. Subsequently, the introduction of permanent porosity emerged as a crucial driving force for further progress in CPOS research. In 2018, Ben *et al.* achieved a significant breakthrough by creating a series of organic salts with permanent porosity using different organic acids and organic bases and proposed the concept of CPOSs for the first time.[26] Taking into consideration the aforementioned content, it becomes paramount to provide a precise and distinct definition of CPOSs, in order to effectively differentiate it from other porous materials. Consequently, we here present the definition of CPOSs, which refers to extended periodic structures with permanent porosity, self-assembled from organic acid and base building blocks through ionic bonds.

Due to the formation of ionic bonds, the presence of charge-separated nano-confined channels, and the inherent ease of preparation and regeneration, CPOSs have attained widespread research interest. Since then, CPOSs have experienced rapid development. Through further in-depth investigations, CPOSs with diverse structures and distinctive functionalities have been synthesized, showcasing extensive application prospects in various domains of fundamental research areas.[29] Such achievements have broadened the horizons of fundamental research and presented promising prospects for the practical application of CPOSs, ultimately shaping a future brimming with possibilities for CPOSs.

CPOSs have undergone a period of development and achieved some accomplishments. However, CPOSs are still in a relatively early stage of development, significantly lagging behind crystalline porous organic materials such as COFs and HOFs. This is primarily due to the shorter development duration for CPOSs, resulting in a limited range of varieties and functionalities. Nevertheless, it also implies that CPOSs hold greater potential for future advancements. Additionally, similar to zeolites, CPOSs possess polar channels and show promising prospects for further industrial applications. Therefore, it is imperative to summarize the development of CPOSs and initiate a fresh evaluation of this burgeoning field.

This review focuses on the synthetic strategies, structural characteristics, application scenarios, and future development prospects of CPOSs. The purpose is to provide scholars in the CPOS field with the latest research trends and directions and to offer valuable insights and guidance to scientists and engineers in related fields.

2. Synthetic strategy

CPOSs are a novel class of crystalline porous organic materials constructed through ionic bonding between organic acids and organic bases, exhibiting permanent porosity. However, the majority of organic salts composed of organic acids and organic bases exhibit poor stability, as the framework readily collapses upon the removal of guest molecules, thus lacking permanent porosity. Consequently, achieving the controlled synthesis of stable CPOSs poses a significant challenge. Considering the reported CPOSs, we have summarized their synthetic strategies, primarily focusing on tectons, acidity/basicity, and topology.

2.1 Tectons

''Tectons'', known as building blocks, serve as the foundation for constructing CPOSs. The term ''tectons'' originated from Greek and was initially proposed by Wuest and colleagues,[69–71] referring to any molecule whose interactions are governed by specific binding forces, thereby inducing the self-assembly of organized networks with particular structures or functional features.[72] Hence, the geometry, size, rigidity, planarity, symmetry,

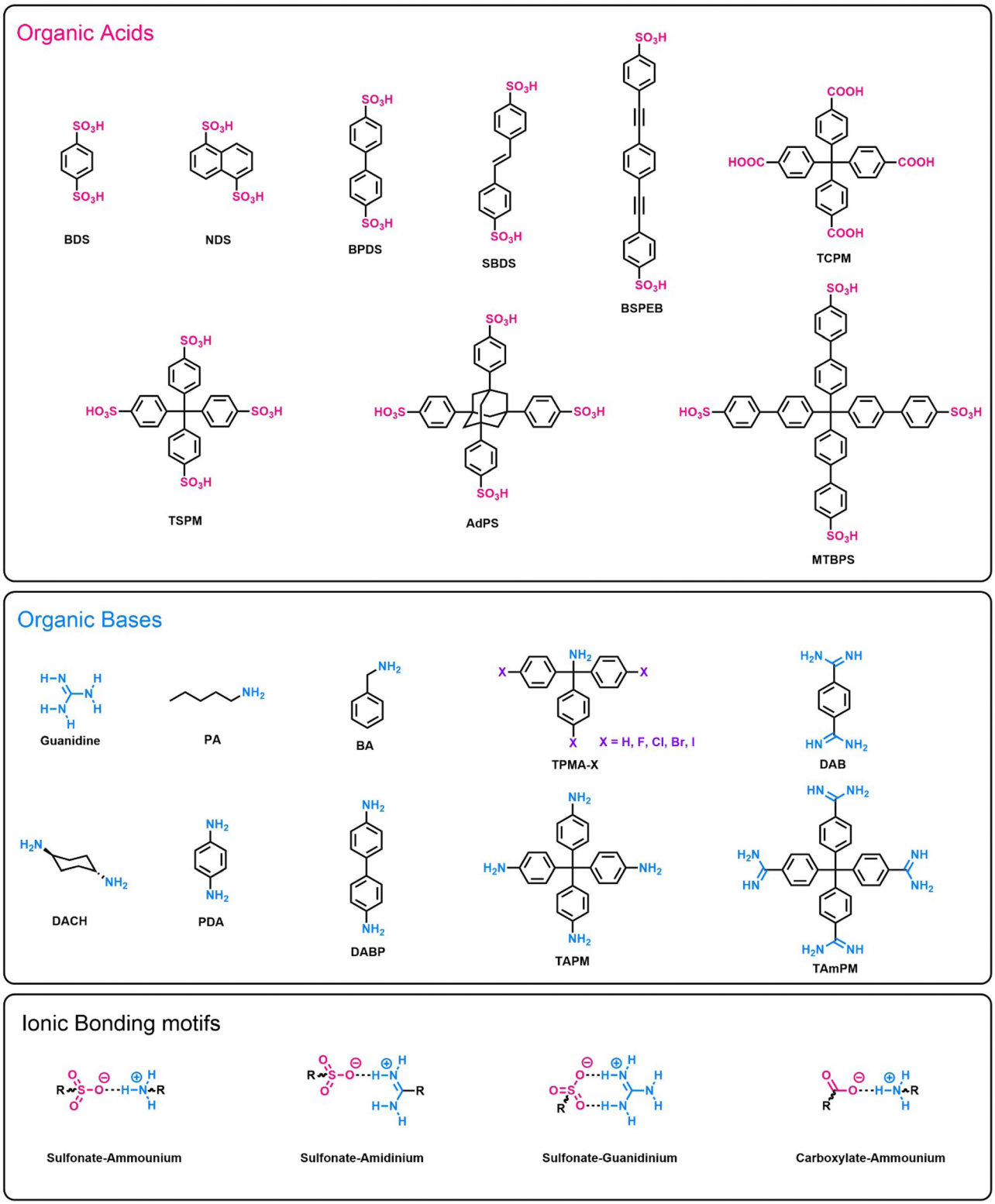

Fig. 1 Schematic representation of organic acids, organic bases and ionic bonding motifs for the construction of CPOSs.

and functionality of tectons are crucial for constructing stable CPOSs.[73] Currently, organic acid mainly involves organic sulfonic acid tectons and organic carboxylic acid tectons. In contrast, organic bases predominantly include organic amino tectons, organic amidine tectons, and organic guanidine tectons (Fig. 1). Different types of patterns, such as sulfonate–ammonium salts, sulfonate–amidinium salts, sulfonate–guanidinium salts, and carboxylate–ammonium salts, can be formed through ionic bonding

between diverse organic acids and organic bases (Fig. 1). Therefore, through the rational design and selection of tectons, it is possible to effectively construct CPOSs.

2.2 Acidity/basicity

The acidity/basicity of tectons, which can be described by pK_a, plays a crucial role in the synthesis of CPOSs. In the field of pharmaceuticals, it is commonly accepted that when ΔpK_a (ΔpK_a = pK_a (base) − pK_a (acid)) is greater than 3, the reaction between an acid and a base is expected to yield a salt.[74–76] Here, we have summarized the ΔpK_a values of the reported CPOSs in Table 2, and the pK_a values were calculated using the predictor functionality in SciFinder, using the program Advanced Chemistry Development (ACD/Labs).[77] The ΔpK_a values of these CPOSs fall within the impressive range of 6.75–14.92, all surpassing the threshold of 3, which unequivocally confirms the formation of salts.

CPOSs are self-assembled from organic acids and organic bases, and the strength of the ionic bonds between them depends, to some extent, on the acidity/basicity of the organic tectons. Thus, the modulation of acidity/basicity is beneficial for improving the stability of CPOSs. For instance, when using similar sulfonic acid and carboxylic acid tectons and reacting them with the same organic base, Ben *et al.* synthesized the structurally similar CPOSs, CPOS-1 and CPOS-4, which exhibited different stabilities.[26] The pK_a difference (ΔpK_a) between tetrakis(4-sulfophenyl)methane (TSPM, pK_a = −1.45) and *trans*-1,4-diaminocyclohexane (DACH, pK_a = 10.78) was 12.23, and CPOS-1 prepared from these two tectons demonstrated excellent stability, withstanding temperatures up to 375 °C. On the other hand, the ΔpK_a between tetrakis(4-carboxylphenyl)methane (TCPM, pK_a = 3.45) and DACH (pK_a = 10.78) was 7.33, resulting in the relatively poor stability of CPOS-4. Moreover, when the ΔpK_a value is below a certain threshold, CPOSs cannot be obtained. For instance, the ΔpK_a between TCPM (pK_a = 3.45) and *p*-phenylenediamine (PDA, pK_a = 6.08) was 2.63, indicating weak interactions between the acids and bases resulting in the inability to form a CPOS. This strategy effectively addresses the synthesis and stability issues of CPOSs, providing valuable guidance for synthesizing new CPOSs.

However, a high ΔpK_a value does not necessarily guarantee the formation of CPOSs with permanent porosity, as it also involves the activation process. Due to the solubility issues of tectons, highly polar solvents (Table 2), such as water or methanol, are usually employed for the synthesis of CPOSs. However, this choice of solvents always brings strong interactions between the often-polar crystallization solvents and the highly charged framework.[35] Organic salt networks formed by sulfonic acids and guanidine, and carboxylic acids and amidines also exhibit significant ΔpK_a values. Nevertheless, many of these systems have yet to be verified to possess permanent porosity.[56,78] Therefore, enhancing the acidity/basicity of the organic tectons and increasing the ΔpK_a represents only one effective approach to preparing stable CPOSs.

2.3 Topology

The tremendous success of reticular chemistry in precisely constructing COFs and MOFs has sparked great interest among scientists in CPOSs.[79,80] Through meticulous analysis of published CPOS structures, we have discovered that reticular chemistry also plays a significant role in the design of CPOSs (Fig. 2(a)). For instance, Ben *et al.* utilized TSPM with T_d symmetry and DACH with C_2 symmetry to synthesize CPOS-1, which exhibits a diamond (*dia*) topology.[26] The combination of TSPM and *p*-phenylenediamine (PDA, C_2 symmetry) generates CPOS-2 with a *dia* topology.26 Replacing the TSPM in CPOS-1 with TCPM (T_d symmetric) yields CPOS-4 with a *dia* topology.[26] Upon selecting a two-node organic base, namely 1,4-diamidiniumbenzene (DAB), possessing C_2 symmetry, reacted with TSPM, CPOS-5 with a *dia* topology was also successfully constructed.[27] Furthermore,

Table 2 Summary of reported CPOSs with different ΔpK_a values

CPOSs	pK_a of organic acids[a]	pK_a of organic bases[a]	ΔpK_a	Crystallization solvents	Ref.
CPOS-1	TSPM (−1.45 ± 0.50)	DACH (10.78 ± 0.70)	12.23	MeOH	26
CPOS-2	TSPM (−1.45 ± 0.50)	PDA (6.17 ± 0.10)	7.62	MeOH/H_2O	26
CPOS-3	TSPM (−1.45 ± 0.50)	DABP (4.70 ± 0.10)	6.15	MeOH/H_2O	26
CPOS-4	TCPM (3.45 ± 0.10)	DACH (10.78 ± 0.70)	7.33	MeOH/H_2O/NaOH	26
CPOS-5	TSPM (−1.45 ± 0.50)	DAB (10.77 ± 0.50)	12.22	THF/H_2O/NaOH	27
CPOS-6	TSPM (−1.45 ± 0.50)	TAmPM (12.20 ± 0.50)	13.65	MeOH/H_2O	30
CPOS-7	TSPM (−1.45 ± 0.50)	TAPM (5.75 ± 0.25)	7.20	THF/GAA	35
d-POS-1	SBDS (−0.87 ± 0.50)	TPMA (7.77 ± 0.10)	8.64	MeOH/*o*-chlorotoluene	31
TPMA/MTBPS	MTBPS (−1.22 ± 0.50)	TPMA (7.77 ± 0.10)	8.99	1,2,4-TCB/DMF	32
TPMA-F/MTBPS	MTBPS (−1.22 ± 0.50)	TPMA-F (7.45 ± 0.10)	8.67	Mesitylene/MeOH	32
TPMA-Cl/MTBPS	MTBPS (−1.22 ± 0.50)	TPMA-Cl (6.90 ± 0.10)	8.12	Benzonitrile/DMAc	32
TPMA-Br/MTBPS	MTBPS (−1.22 ± 0.50)	TPMA-Br (6.90 ± 0.10)	8.12	Benzonitrile/DMAc	32
AdPS/TPMA-Cl	AdPS (−1.05 ± 0.50)	TPMA-Cl (6.90 ± 0.10)	7.95	MeOH	33
AdPS/TPMA-Br	AdPS (−1.05 ± 0.50)	TPMA-Br (6.90 ± 0.10)	7.95	MeOH	33
AdPS/TPMA-I	AdPS (−1.05 ± 0.50)	TPMA-I (7.01 ± 0.10)	8.06	MeOH	33
BSPEB/PA	BSPEB (−1.12 ± 0.50)	PA (10.69 ± 0.10)	11.81	MeOH/1,4-dioxane	37
BSPEB/BA	BSPEB (−1.12 ± 0.50)	BA (9.06 ± 0.10)	10.18	MeOH/1,4-dioxane	38
HOF-GS-10	NDS (−0.60 ± 0.40)	Guanidine (13.27 ± 0.70)	13.87	MeOH/Acetone	36
HOF-GS-11	BPDS (−1.14 ± 0.50)	Guanidine (13.27 ± 0.70)	14.41	MeOH/*p*-xylene	36
p-G_2BDS	BDS (−1.65 ± 0.50)	Guanidine (13.27 ± 0.70)	14.92	MeOH/acetone	34

[a] Calculated using Advanced Chemistry Development (ACD/Labs) Software V11.02 (©1994–2023 ACD/Labs).

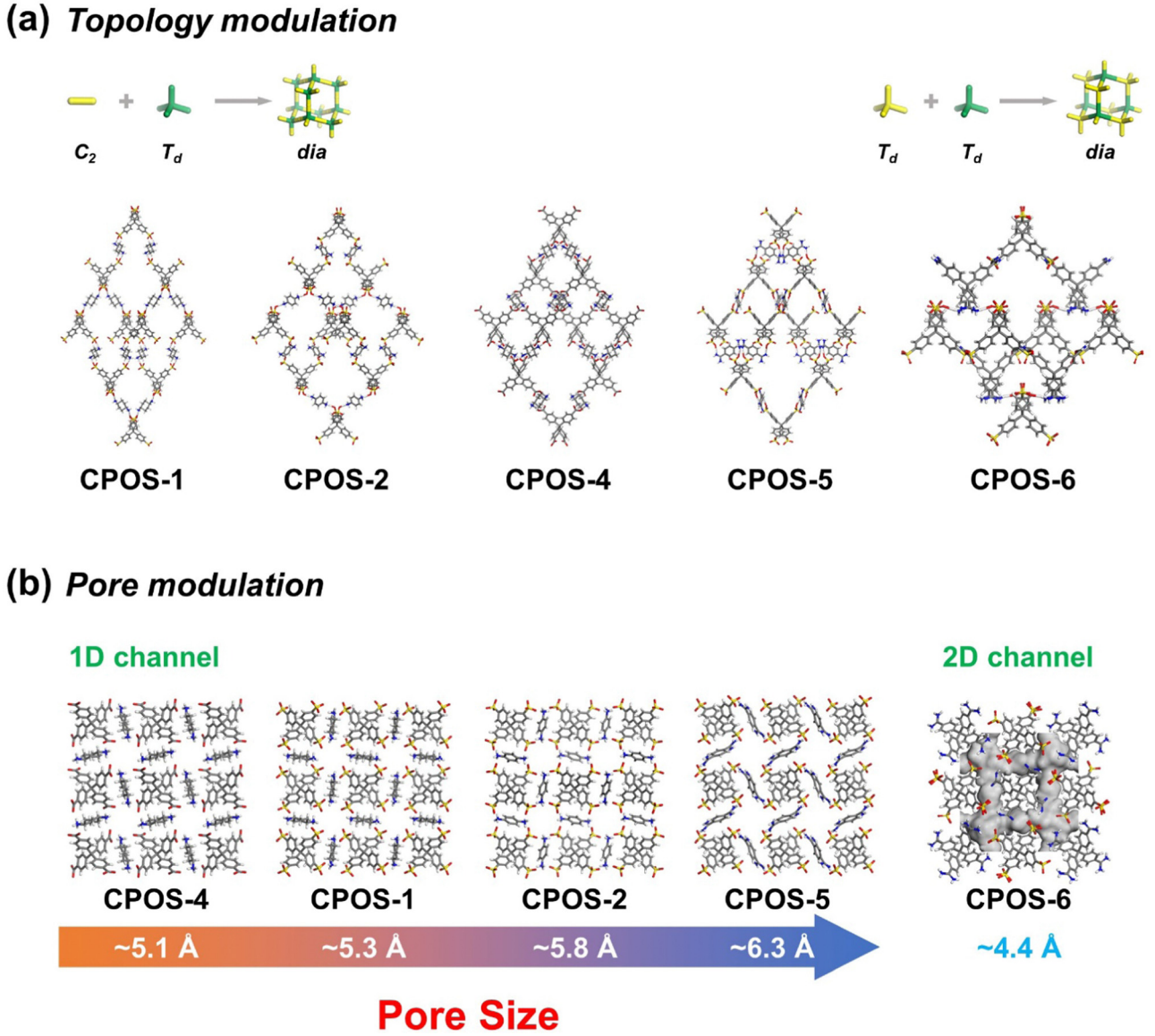

Fig. 2 (a) Topology modulation of CPOSs. (b) Pore modulation of CPOSs.

employing TSPM and tetrakis(4-amidinophenyl)methane (TAmPM), both four-node tectons with T_d symmetry, CPOS-6 with a *dia* topology was also achieved.[30] Intriguingly, CPOS-1, 2, 4, 5, and 6 all exhibit *dia* topology, while their pore dimensions and sizes can be modulated through acid/base building blocks (Fig. 2(b)). CPOS-1, 2, 4, and 5, constructed with building blocks derived from T_d and C_2 symmetries, possess 1D pore channels, whereas CPOS-6, built from two T_d-symmetric building blocks, presents 2D pore channels. With the increase in the length of the organic bases, the pore diameter of CPOS-1, 2, and 5 can be precisely and effectively modulated, ranging from 5.3 to 6.3 Å. These explicit sub-nanometer channels enable CPOSs to have potential applications in the construction of biomimetic ion channels.

Here, it is worth mentioning that Tohnai *et al.* successfully constructed tetrahedral stable supramolecular clusters by employing organic sulfonic acids and triphenylmethylamine (TPMA).[60] Subsequently, utilizing the principles of reticular chemistry, it is possible to assemble tetrahedrally stable supramolecular clusters into CPOSs with *dia* topology using the rational design of organic acids.[31–33] Furthermore, the introduction of halogen atoms onto TPMA also led to the formation of alternative topological structures in CPOSs, such as *sod* topology.[33] Hence, reticular chemistry can predict the topology of CPOSs to some extent. However, due to the flexible and non-directional nature of ionic bonds, accurately predicting their crystal structures, similar to the case of COFs, remains highly challenging.

3. Characteristics

CPOSs, as a unique class of crystalline porous materials, form charge-separated highly polar nano-confined channels and

highly ordered permanent porous structures through ionic bonding. The presence of ionic bonds distinguishes CPOSs from other porous organic materials and imparts excellent stability to their frameworks. The distinctive high-polarity channels in CPOSs resemble zeolite and possess highly confined characteristics, greatly expanding the applications of CPOSs. The permanent porosity of CPOSs implies that the pore structure remains intact and open after the removal of guest molecules, providing favorable conditions for exploring host–guest chemistry. In the following sections, we will discuss the characteristics of CPOSs in detail from three perspectives: ionic bonding, charge-separated highly polar nano-confined channels, and permanent porosity.

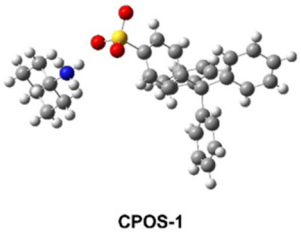

Interaction	Energy (kJ/mol)
Electrostatics	-387.03
Exchange	42.72
Induction	-52.21
Dispersion	-17.82
Total	-414.35

Fig. 4 Molecular fragments of CPOS-1 and the interaction energy between organic acid and organic base.

3.1 Ionic bonds

The ionic bond, as a crucial strong non-covalent interaction in CPOSs, is flexible and non-directional, playing a predominant role in maintaining the structural integrity of CPOSs. However, in most CPOSs, the formation of ionic bonds is often accompanied by the formation of hydrogen bonds, which are weak, non-covalent interactions with directionality that only have an auxiliary role in the construction of CPOSs. For instance, CPOS-1 without guest molecules (denoted as CPOS-1-dried) exhibits NLC behaviour under high pressure.[28] As illustrated in Fig. 3, when the pressure increased from 0.0001 to 2.32 GPa, the hydrogen bond length shrank, indicating an increase in the salt-bridge interactions. It demonstrates that ionic bonds under high pressure can maintain structural integrity, emphasizing the irreplaceable role of ionic bonds in maintaining the stability of CPOSs. Furthermore, in the case of CPOS-6, directional hydrogen bonds are disrupted during phase transition, while flexible and non-directional ionic bonds are responsible for maintaining the integrity of the framework.[81]

We conducted relevant theoretical calculations to further confirm the dominant role of ionic bonds in CPOSs. By extracting the organic acid–base molecular fragments from the CPOS structure, we employed the symmetry-adapted perturbation theory (SAPT) calculations using the PSI4 program to evaluate the interactions between the organic acid and organic base. As shown in Fig. 4, the interactions between organic acids and bases primarily involve electrostatic, exchange, induction, and dispersion forces. The total energy is -414.35 kJ mol^{-1}, which can be considered as the sum of hydrogen bond and ionic bond energies. To reduce the interaction between ions, we have built a model system in which the fragments were modified to be neutral. In the neutral model, the electrostatic interaction energy is reduced to -23.63 kJ mol^{-1}, and the change in other interactions is negligible. The sum of all interactions in the

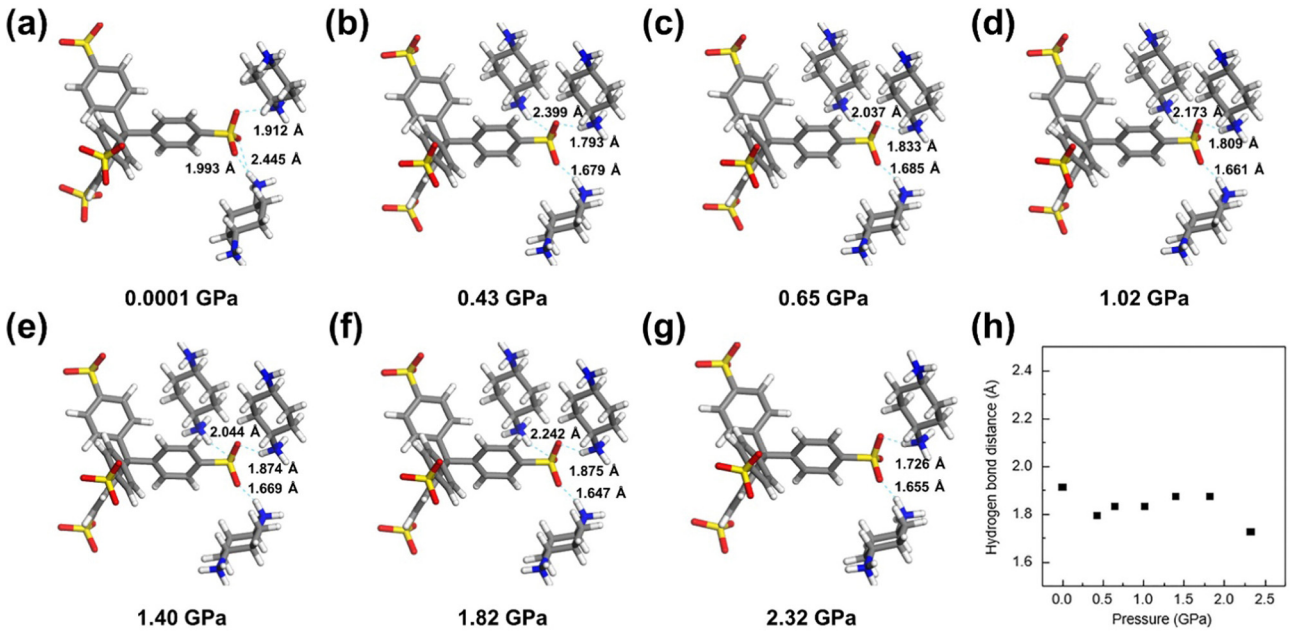

Fig. 3 (a)–(g) Crystal structure of CPOS-1-dried under different pressure. (h) Hydrogen bond distance changes with increasing pressure in CPOS-1-dried. Reproduced with permission.[28] Copyright 2020 American Chemical Society.

neutral model system is approximately -50.94 kJ mol^{-1}, which can be considered as the energy of hydrogen bonds. Hence, we can estimate the energy of the ionic bond as the difference between the electrostatic interaction energy in the charged state and the neutral state, with a value of -363.40 kJ mol^{-1}. It is obvious that both hydrogen and ionic bonds contribute electrostatic interaction energy, but hydrogen bonds only provide a minor contribution. Hence, ionic bonds occupy the dominant position among electrostatic interactions. In other words, the interactions between organic acids and organic bases are primarily ionic bonds. Consequently, we prefer to refer to this class of materials as CPOSs rather than HOFs. This distinction has significant importance for understanding the fundamental interactions within CPOSs.

The presence of ionic bonds imparts unique physical and chemical properties to CPOSs, along with enhanced structural stability. It is possible to achieve precise control over ionic bonds and optimize the performance of porous materials through appropriate structural design and control, thus expanding their application scope and functionalities.

3.2 Charge-separated highly polar nano-confined channels

During the formation of CPOSs, proton transfer typically occurs between organic acids and organic bases,[82] resulting in the organic acid losing a proton and acquiring a negative charge. In contrast, the organic base gains a proton and carries a positive charge. After the formation of CPOSs, the deprotonated organic acids, and protonated organic bases arrange themselves in a regular pattern within the pores, leading to charge separation.

For instance, CPOS-5 exhibits a channel formed by acid–base functionalities. The charges are arranged in a regular pattern within the pore channels, giving rise to channels with double helices of electrostatic charges.[27] Furthermore, both the organic acids and organic bases possess polar functional groups and are uniformly distributed on the surface of the CPOS channels. This imparts a high polarity to the surface, enhancing the adsorption capacity and selectivity of CPOSs towards polar substances. In addition, the charge-separated highly polar nano-confined channels of CPOSs, which typically exist at the sub-nanometer scale and resemble biological channels, exhibit remarkable confinement properties, enabling the efficient adsorption, separation, storage, and transportation of substances. Therefore, the presence of charge-separated highly polar nano-confined pores provide CPOSs with broad potential applications in various areas, such as proton conduction and rapid transport of guest molecules/ions. Furthermore, precise control over the pore structure and surface chemistry of CPOSs allows for accurate manipulation of adsorption and selective separation, thereby expanding the application scope of CPOSs to meet diverse needs across different fields.

3.3 Permanent porosity

A plethora of crystalline organic salts with porous structures can be formed using organic acids and bases. However, some organic salts may collapse into amorphous or dense phases after removing guest molecules from the pores, resulting in a loss of porosity. Such materials are referred to as crystalline organic salt networks. Only organic salts with permanent porosity can be classified as CPOSs, which represents a crucial characteristic of CPOSs. However, obtaining organic salts with permanent porosity remains a significant challenge. The strong interaction between solvents and frameworks within the pores makes it only possible for a few highly stable organic salts to achieve permanent porosity through a direct heating activation method. To overcome this issue, employing appropriate activation methods to remove embedded guest molecules under mild conditions (*e.g.*, solvent exchange, supercritical CO_2 extraction, *etc.*), could potentially serve as feasible approaches to obtaining CPOSs with permanent porosity.

The permanent porosity endows CPOSs with extensive application potential in many fields. With precise control over their structure and functionality, CPOSs can be utilized for selective adsorption, separation of specific molecules, catalytic reactions, *etc.* Furthermore, CPOSs can be designed and tailored according to specific requirements, expanding their application scope and enhancing their performance.

Gas adsorption is a common and effective method to characterize the permanent porosity of CPOSs. Typically, the porosity of porous materials is assessed using N_2 (3.64 Å) as a probe at 77 K under standard conditions. However, N_2 is not completely inert, and the charged-separated polar channels of CPOSs tend to polarize N_2 molecules, leading to quadrupole interactions that hinder accurate characterization of porosity using N_2. Additionally, N_2 adsorption is inaccurate for quantifying micropores, especially ultramicropores (<7 Å), making it inadvisable for CPOS porosity characterization.

On the other hand, carbon dioxide (CO_2) with a smaller kinetic diameter (3.30 Å) is a highly effective probe for analyzing micropores smaller than 1 nm, making it a suitable choice. Currently, the main method for characterizing the porosity of CPOSs relies on CO_2 adsorption although CO_2 is also easily polarized.[83] For instance, CO_2 adsorption is measured at 273 K to generate an adsorption isotherm, and the surface area is calculated using the Dubinin–Astakhov (DA) method,[26] or CO_2 adsorption is tested at 195 K for surface area calculation using the Brunauer–Emmett–Teller (BET) method.[31] However, the surface area results obtained from different conditions are not comparable, making it necessary to develop a unified method for characterizing the porosity of CPOSs.

At 273 K, CO_2 diffusion is rapid, enabling it to enter pores smaller than 0.4 nm. A high-resolution micropore distribution profile can be obtained by employing DFT calculations. Considering that the pores of CPOSs primarily fall into the ultramicropore range, it is recommended to test CO_2 adsorption isotherms at 273 K and employ DFT calculations to determine the surface area and pore size distribution of CPOSs.

4. Applications

The presence of ionic bonds, charge-separated highly polar nano-confined channels, and permanent porosity gives CPOSs unique physicochemical properties, providing a broad platform for exploring host–guest interactions and applications. The

existence of ionic bonds brings forth distinctive properties in the CPOS framework, allowing for changes in the spatial positions of both the framework and guest molecules under external stimuli, such as NLC. The highly polar nature of CPOS channels enables the accommodation of highly polar molecules, such as water molecules, and facilitates proton conduction. Additionally, the charge separation and nano-confined characteristics of the channels result in the polarization of guest molecules, allowing for the rapid transport of molecules/ions, such as the rapid transport of CO_2 molecules, selective and rapid transport of K^+, and efficient AWH. The presence of permanent porosity allows for the adsorption of diverse guest molecules, leading to spatial interactions between guests and the host framework, enabling applications such as gas sorption, molecular rotors, fluorescence modulation, RTP and catalysis.

Stability is another critical consideration when utilizing CPOSs. Although CPOSs possess exceptional thermal stability, their chemical stabilities are relatively low, rendering them vulnerable to dissolution in highly polar solvents and incapable of withstanding strong acid or alkali conditions. Nevertheless, this feature also allows for relatively easy regeneration of CPOSs, endowing them with numerous advantages such as sustainability, environmental-friendliness, and economic viability throughout their application process. In this section, we summarize the current applications of CPOSs and discuss their utilization in various fields.

4.1 Negative linear compression

NLC refers to the phenomenon where materials exhibit volume shrinkage while simultaneously expanding in a specific direction under pressure. It is an extraordinary and rare high-pressure structural behaviour with significant applications in fields such as ultra-sensitive pressure sensors, artificial muscles, and optical fibers.[84–86] CPOSs, with their flexible and non-directional stable ionic bonds, can be used to construct highly compressible topological structures, thereby converting extreme compressibility into NLC behaviour. In 2020, Ben *et al.* discovered the *dia* topological structure in CPOS-1 (Fig. 5(a)) and identified the presence of "supramolecular springs" composed of sulfonate anions and ammonium cations distributed along the *a* and *b* axes (Fig. 5(b)).[28] At the molecular scale, the compressibility of these springs is infinitely amplified under high pressure due to the cumulative effect of the helix. Therefore, CPOS-1 exhibits a remarkable NLC behaviour along the *c*-axis direction, with high negative compressibility of $K_c = -90.7\ TPa^{-1}$ (Fig. 5(c)). Furthermore, the pressure-induced NLC behavior leads to the gradual elongation of the 1D helical water chain within CPOS-1 along the *c*-axis direction, eventually causing the chain to break, resulting in an increase in electrical resistance along the *c*-axis direction from $1.74 \times 10^8\ \Omega$ (ambient pressure, 300 K) to $3.28 \times 10^8\ \Omega$ (16.01 GPa) (Fig. 5(d)). The unique framework stability and variations in the spatial arrangement of the framework and guest molecules under high pressure offer new insights for designing materials with excellent NLC performance.

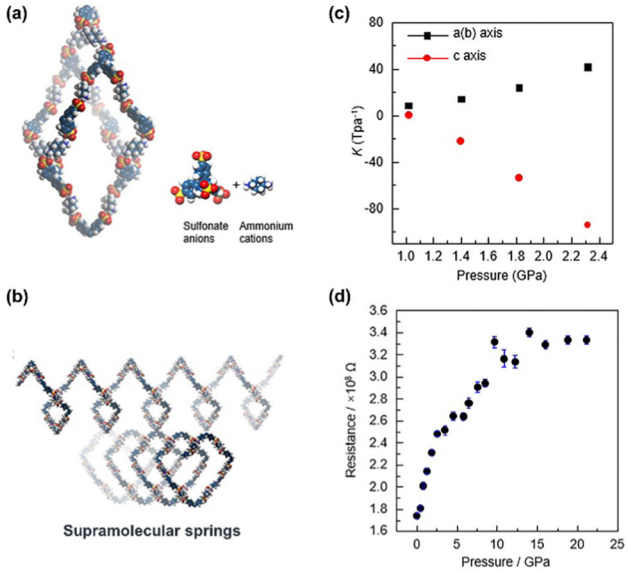

Fig. 5 (a) Diamond topology network of CPOS-1. (b) The "supramolecular spring" network formed along mutually perpendicular *a* and *b* axes. (c) Pressure-dependent compressibility of CPOS-1-dried. (d) Pressure-dependent single crystal electrochemical impedance spectroscopy of water@CPOS-1. Reproduced with permission.[28] Copyright 2020 American Chemical Society.

4.2 Proton conduction

Proton exchange membrane fuel cells (PEMFCs) are fuel cells that use proton-conductive materials as electrolytes. They have advantages such as fast start-up, high power density, and good stability, making them ideal energy sources for future applications in automobiles, aerospace, portable power, and other fields.[87] The performance of PEMFCs heavily relies on the proton conductivity of the proton exchange membrane (PEM), which is a crucial component in PEMFCs. Currently, the most researched and widely applied commercial PEM is Nafion produced by DuPont. It exhibits high proton conductivity at room temperature in the presence of water. However, complex preparation processes, high production costs, and durability issues hinder the development of Nafion membranes.[88] Furthermore, the amorphous nature of Nafion makes it challenging to study proton conduction mechanisms and control proton transport pathways at the molecular level. In comparison, CPOSs offer the following advantages as proton conductive materials: (1) The channels possess high polarity, allowing for the accommodation of highly polar water molecules, facilitating proton conduction; (2) the pores contain acidic functional groups that can dissociate and generate a large number of protons, thus increasing proton conductivity; (3) CPOSs have a tailored structure, good stability, simple synthesis methods, and can be manufactured on a large scale. Hence, CPOSs represent an ideal choice for proton-conductive materials and possess potential applications in the PEMFC field.

In 2016, Ghosh *et al.* synthesized two CPOSs (GS-HOF-10 and GS-HOF-11) using aromatic groups as support pillars and guanidinium sulfonate (GS) moieties as roofs.[36] These two

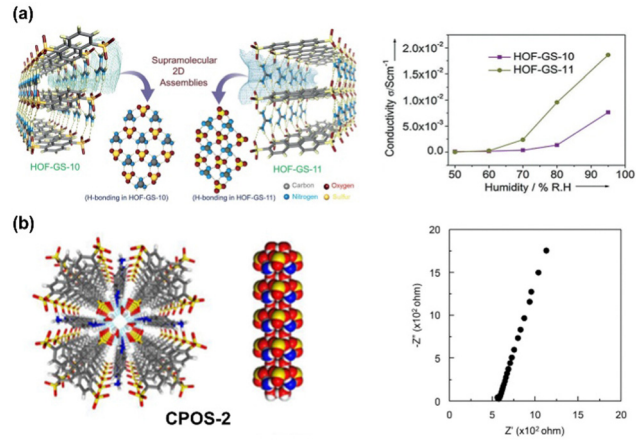

Fig. 6 (a) The structures and proton conductivities of HOF-GS-10 and HOF-GS-11, respectively. Reproduced with permission.[36] Copyright 2016 Wiley-VCH. (b) The structure and proton conductivity of CPOS-2. Reproduced with permission.[26] Copyright 2018 Wiley-VCH.

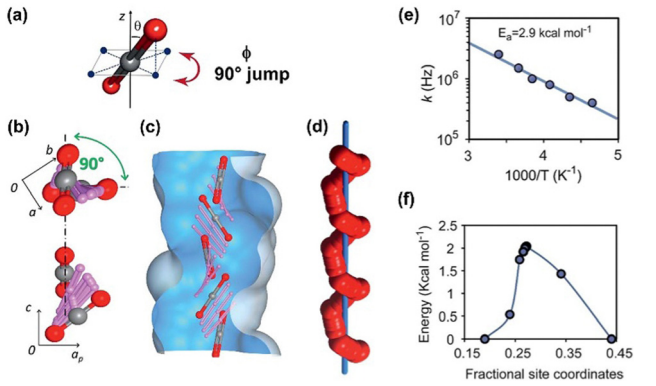

Fig. 7 (a) Inclination angle of the CO_2 main axis with respect to the reorientation-axis *z* about which the 90° jump occurs. (b) Screwing mechanism for CO_2 rototranslational dynamics in the channel. (c) Overlay of the CO_2 positions along the channel as calculated using the DFT transition state method. (d) Helical trajectory of one CO_2 oxygen atom (red spheres) about the channel axis (blue bar). (e) Arrhenius plot of the reorientational rates (*k*) *versus* the inverse of temperature. (f) The calculated energy profile for the rototranslation of CO_2 along the channel. Reproduced with permission.[27] Copyright 2019, Royal Society of Chemistry.

materials exhibited sufficient stability and maintained crystallinity even at 320 °C. Moreover, because of the highly polar and acidic nature of the pores, these materials were applied for proton conduction and GS-HOF-11 demonstrated a high proton conductivity of up to 10^{-2} S cm^{-1} under high humidity conditions (Fig. 6(a)). Subsequently, in 2018, Ben *et al.* successfully prepared four CPOSs (CPOS 1–4) using two organic acids and three organic bases.[26] Among them, CPOS-2, with highly polar channels, accommodated the largest number of water molecules. The sulfonic groups within its structure could dissociate and release a large number of protons, resulting in the highest proton conductivity (Fig. 6(b)). At 60 °C and 98% relative humidity (RH), the proton conductivity of CPOS-2 reached a remarkable 2.2×10^{-2} S cm^{-1}, making it one of the best-performing porous materials in terms of proton conductivity reported at the time. The activation energy calculated using the Arrhenius equation was greater than 0.4 eV, indicating proton transport following the vehicular mechanism where water molecules serve as carriers for proton transportation within the channels. Additionally, powder X-ray diffraction (PXRD) showed no significant changes after proton conduction measurements, indicating the excellent stability of CPOSs. Subsequently, the same research group introduced non-volatile acids (H_2SO_4 and H_3PO_4) into CPOS-1 to increase the content of protons, and the obtained materials showcase outstanding proton conductivities, which provides an effective strategy to enhance the proton conductivity of CPOSs.[89] These studies demonstrated the significant advantages and broad application prospects of CPOSs in the field of proton conduction.

4.3 Rapid transport of CO_2 molecules

CPOSs possess polar nano-confined channels with charge separation, analogous to protein channels found in biological systems, bearing significant advantages in facilitating the rapid transport of guest molecules. For example, CPOS-5 with sub-nanometer dual helical electrostatic channels exhibited remarkable selectivity towards CO_2 molecules.[27] Solid-state nuclear magnetic resonance (ssNMR) spectroscopy revealed that CO_2 molecules can rapidly flip 90° within the channels, moving from one site to another helically with a transfer rate as high as one million steps per second (10^6 steps per s) (Fig. 7(a)–(d)). Moreover, the activation energy for this transmission process is merely 2.1 kcal mol^{-1} (Fig. 7(e)) which is consistent with the theoretical calculation (Fig. 7(f)). This research achievement has unveiled the crucial role of sub-nanometer double-helical electrostatic channels in facilitating the rapid transport of guest molecules, challenging the general rule of thumb that narrower pore size leads to slower kinetics. It also provides valuable insights for the design and synthesis of bio-inspired porous materials with special transport channels.

4.4 Selective and rapid transport of K^+ ions

Ion channels in biological systems enable rapid and selective transmembrane transport of specific ions, playing a crucial role in chemical reactions and information transfer.[90–92] The potassium ion channel, KcsA, is a common example of a biological ion channels (Fig. 8(a)), characterized by angstrom-scale dimensions and abundant surface binding sites that facilitate highly efficient and selective transport of K^+ ions (transporting 10^8 potassium ions per second with a K^+/Na^+ selectivity ratio of 10^4).[93] CPOSs possess charge-separated sub-nanometer confinement channels that closely resemble the KcsA found in living systems. Therefore, the utilization of CPOSs to construct bio-inspired ion channels resembling KcsA shows promise for achieving the highly efficient and selective separation of K^+ ions.

In 2022, Wen *et al.* achieved *in situ* growth of CPOS-5 within a conical nanochannel, fabricating a bio-inspired KcsA channel (Fig. 8(b)).[94] At the sub-nanometer scale, the conical dual-helical channels exhibited typical ion rectification behaviour (Fig. 8(c)), enabling fast K^+ transport at a rate of 94.4 mmol m^{-2} h^{-1} (Fig. 8(d)). Moreover, the synergistic effect of cation–π and

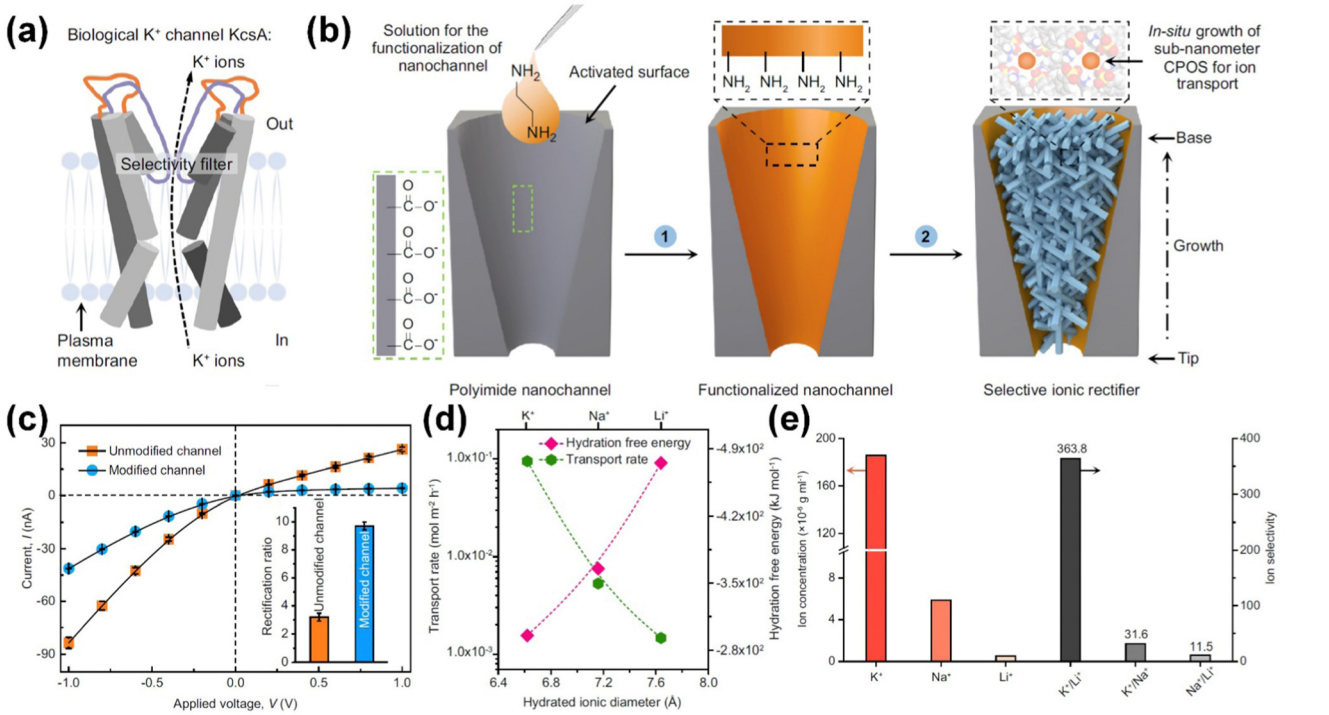

Fig. 8 (a) KcsA K^+ channels embedded in the plasma membrane. (b) Schematic showing the preparation and incorporation of the CPOS into conical transmembrane nanochannels. (c) *I*–*V* curves of the conical nanochannel before (orange) and after (blue) CPOS growth, respectively. (d) Experimental ion transport rate as a function of the hydration ionic diameter and hydration free energy, respectively. (e) A comparison of the ion concentration in the permeation compartment (left) and ion selectivity in the CPOS channels was obtained by calculating the ion concentrations ratios in the permeation compartment (right). Reproduced with permission.[94] Copyright 2022 Nature Publishing Group.

electrostatic interactions raised the energy barrier for Li^+ and Na^+ ions, resulting in the selective transportation of K^+ ions. The selectivity ratios of K^+/Li^+ and K^+/Na^+ reached 363 and 31, respectively (Fig. 8(e)). This study opens new avenues for the design of novel bio-inspired ion channels.

4.5 Atmospheric water harvesting

With the rapid growth of the world's population, the scarcity of water resources has become an increasingly severe and significant global issue. While desalination technology can effectively increase the freshwater supply, it is restricted to coastal areas and has obvious geographical limitations. The utilization of porous materials for AWH is an important approach to alleviate freshwater shortages.[95–99] CPOSs feature highly polar nanochannels formed by organic acids and bases, exhibiting excellent hydrophilicity and have the potential for efficient AWH.

In 2022, Ben *et al.* synthesized a novel type of CPOS, named CPOS-6, using TSPM and TAmPM (Fig. 9(a)).[30] CPOS-6 demonstrated permanent porosity and possessed highly polar channels capable of capturing water molecules. As shown in Fig. 9(b), CPOS-6 demonstrates an S-shaped water adsorption curve, with a significant increase in water uptake observed in the range of 50 to 60% RH. Additionally, at 313 K, every gram of adsorbent can rapidly release 0.126 g of water within 10 min (Fig. 9(c)). This behaviour can be attributed to the unique dual hydrogen bonding system of CPOS-6 (Fig. 9(d)). Water molecules entering the channels at low RH form strong hydrogen bond interactions with the strongly polar functional groups, while subsequent water molecules entering the channels at a higher RH interact weakly with the pre-existing water molecules through hydrogen bonding. The presence of the dual hydrogen bonding system not only accelerates the adsorption kinetics of water molecules but also allows the weakly bonded water molecules in the desorption process to be released at lower temperatures. Although CPOS-6 exhibits a relatively low single adsorption capacity (0.23 g g^{-1}), its highly polar channels and the dual hydrogen bonding system within the framework structure contribute to its remarkable water production (2.16 g g^{-1} day^{-1}), which surpasses many reported porous materials including MIL-101, SAPO-34 and COF-300 (Fig. 9(e)). As such, it has potential applications in AWH and provides new insights for designing novel and efficient AWH adsorbent materials.

Subsequently, Ben *et al.* discovered that CPOS-6 possesses continuous sub-nanometer confined channels with dimensions approximately twice the kinetic diameter of water molecules (Fig. 10(a)). This characteristic allows water molecules adsorbed within the polar channels to have the lowest van der Waals potential energy, facilitating their rapid transport within the channels and exhibiting the "superfluidic" behaviour of water molecules (Fig. 10(b)).[100] As a result, rapid adsorption and desorption of water can be achieved on a macroscopic scale.

4.6 Gas sorption

The permanent porosity offers a gateway to facilitate gas sorption processes, leading CPOSs to emerge as a promising

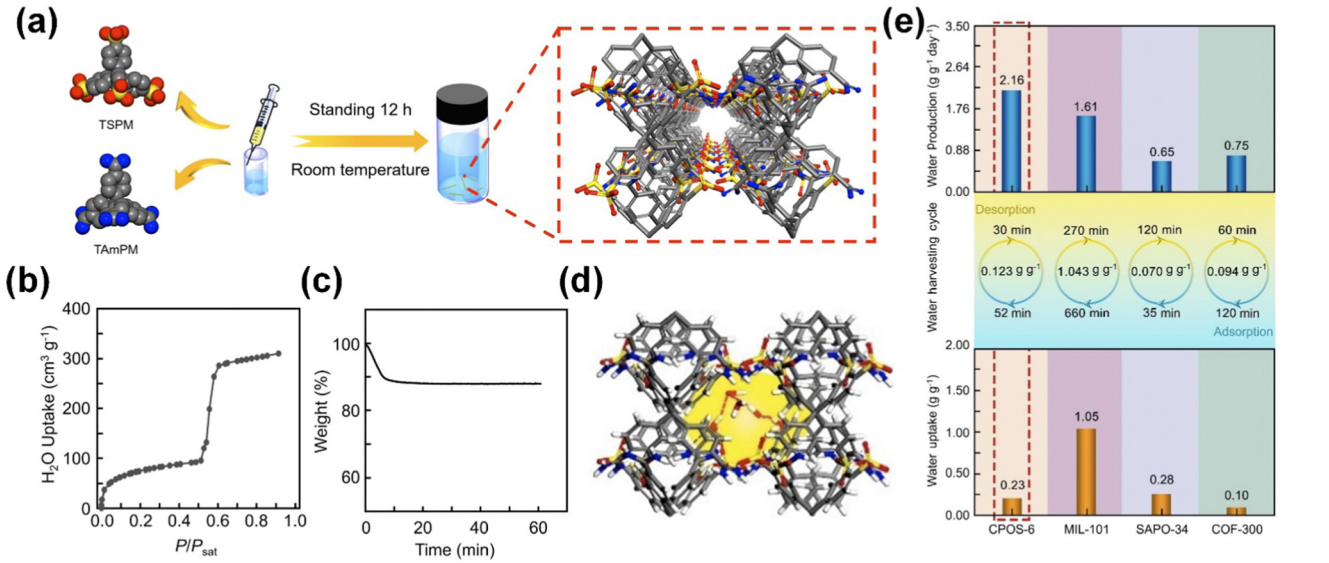

Fig. 9 (a) Schematic of the synthesis of CPOS-6 and its crystal structure. (b) Water vapor adsorption isotherms of CPOS-6 at 298 K. (c) TGA curves of saturated adsorbed CPOS-6 at 45–50% RH and heated to 313 K. (d) Dual hydrogen bond system in CPOS-6. (e) Water adsorption capacities of CPOS-6, MIL-101, SAPO-34, and COF-300 at 70% RH, calculated from the water vapor adsorption isotherms at 298 K (bottom). Water harvesting cycle durations and water production in each cycle for several materials (middle). Expected water production in one day for different materials (top). Reproduced with permission.[30] Copyright 2022 Wiley-VCH.

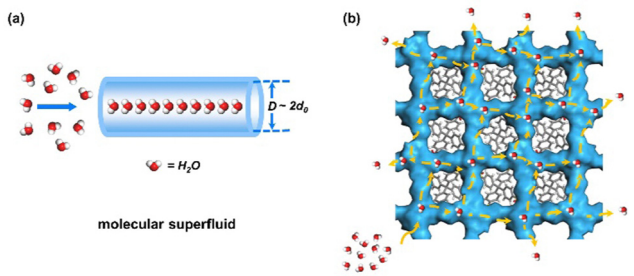

Fig. 10 (a) Water molecules are confined to a nanochannel of a certain diameter to form a molecular superfluid. (b) Continuous pathways and rapid water transport in CPOS-6. Reproduced with permission.[100] Copyright 2023 Wiley-VCH.

Table 3 Summary of gas adsorption capacity of CPOSs

CPOSs	CO_2 uptake ($cm^3\ g^{-1}$)	N_2 uptake ($cm^3\ g^{-1}$)	Ref.
CPOS-1	40 (273 K)	—	26
CPOS-2	27 (273 K)	—	26
CPOS-3	4 (273 K)	—	26
CPOS-4	8 (273 K)	—	26
CPOS-5	48 (273 K)	—	27
CPOS-6	9 (273 K)	—	30
CPOS-7	96 (195 K)	—	35
d-POS-1	87 (194 K)	—	31
TPMA/MTBPS	110 (195 K)	8 (77 K)	32
TPMA-F/MTBPS	182 (195 K)	92 (77 K)	32
TPMA-Cl/MTBPS	115 (195 K)	126 (77 K)	32
TPMA-Br/MTBPS	82 (195 K)	34 (77 K)	32
AdPS/TPMA-Cl	101 (195 K)	—	33
AdPS/TPMA-Br	133 (195 K)	—	33
AdPS/TPMA-I	66 (195 K)	—	33
BSPEB/PA	50 (195 K)	—	37
BSPEB/BA	86 (195 K)	—	38
HOF-GS-10	42 (195 K)	—	36
HOF-GS-11	33 (195 K)	—	36
p-G_2BDS	35 (298 K)	112 (77 K)	34

platform for gas adsorption. However, due to the nature of the channel polarity, most CPOSs exhibit limited affinity towards N_2 adsorption while demonstrating a remarkable propensity for adsorbing CO_2. As shown in Table 3, all the CPOSs display excellent CO_2 adsorption capacity, and only a few CPOSs (*e.g.* TPMA-Cl/MTBPS, *p*-G_2BDS, *etc.*) exhibit N_2 adsorption behaviour. This peculiarity opens up intriguing opportunities for the potential application in capturing and separating CO_2 from gaseous mixtures, potentially contributing to mitigating the adverse impacts of greenhouse gas emissions. For instance, CPOS-5 displays a high CO_2 adsorption of 48 $cm^3\ g^{-1}$ at 273 K and a high isosteric heat of adsorption (Q_{st}) of 34.5 kJ mol^{-1}, demonstrating high affinity toward CO_2 molecules.[27] Hence, CPOS-5 shows a high CO_2/N_2 selectivity value up to 690, which was a benchmark in the field of porous molecular materials at that time.

The gas adsorption behaviour can also be modulated by controlling the void structures and environments of CPOSs. Recently, Tohnai *et al.* successfully synthesized a novel CPOS featuring a resilient diamond network by employing 4′,4‴,4⁗,4⁗′-methanetetrayltetrakis((1,1′-biphenyl)-4-sulfonic acid) (MTBPS) and triphenylmethylamine (TPMA).[32] Through the introduction of substituents at the *para*-positions of the benzene rings in TPMA, CPOSs with substituents exposed on the void surface were successfully prepared. The steric hindrance induced by these exposed substituents caused distortion within the diamond networks of the CPOSs, thereby rendering an interpenetration style in the diamond network of TPMA-X/MTBPS (X = F, Cl, Br, I). This alteration influenced the sizes and shapes of their voids, leading to the formation of a myriad of intricate porous structures. Additionally, it further exerts its

influence on the gas adsorption behaviour. With the electronegativity of the halogen substituent, CPOS from TPMA substituted by fluorine (TPMA-F/MTBPS) exhibits the highest isosteric heat of CO_2 adsorption and high CO_2 adsorption of 182 $cm^3\ g^{-1}$ at 1 atm in all organic porous materials. Very recently, Cooper *et al.* employed a high-throughput screening (HTS) approach to meticulously modify the solvent composition and introduce a dehydration agent, effectively preventing the formation of CPOS hydrated.[35] This innovative methodology led to the discovery of a novel CPOS, namely CPOS-7, consisting of TSPM and tetrakis(4-amino-phenyl)methane (TAPM), boasting remarkable stability and exhibiting an exceptional maximum CO_2 adsorption capacity of 96 $cm^3\ g^{-1}$ at 195 K. The exceptional gas sorption performance of CPOS-7 establishes it as one of the most porous CPOSs hitherto reported.

Since the first report in 1994,[101] salts formed by the guanidinium organosulfonate motif, here denoted as GS salts, have gradually progressively burgeoned into a formidable lineage boasting a vast assemblage exceeding 500 members.[102] However, over an extended period of time, GS-derived salts have been consistently perceived as lacking in permanent porosity. It was not until 2020 that the research conducted by Holman *et al.* finally shattered this stasis. Their research unveiled the first example thus far of GS salts, namely *p*-G_2BDS, exhibiting remarkable gas adsorption behavior.[34] *p*-G_2BDS exhibits fully reversible Type I gas sorption isotherms using N_2 as the gas probe, giving a BET surface area of 408.7 $m^2\ g^{-1}$. Moreover, they also found that the collapsed form of *p*-G_2BDS (denoted as *np*-G_2BDS) can readily be returned to the porous form by applying gas pressure. This represents a significant breakthrough in GS salts, heralding a guiding light for the exploration and discovery of additional porous GS salts.

4.7 Molecular rotors

In recent years, the rapid advancement of molecular machines has propelled molecular rotors into the forefront of research. The strategy to prepare the fast molecular rotors is capping the rotors with large substituents, providing sufficient free volume for rotational motion of rotors. The arrangement of rotors within a material also has a significant impact on its overall properties.[103,104]

Generally, rotors are arranged on the crystal surface or within the bulk crystals in a 2D or 3D fashion.[105] The emergence of crystalline porous materials has presented an exceptional platform for constructing molecular rotors. However, the integration of ordered molecular rotors with porosity remains a formidable challenge. CPOSs offer two distinctive advantages in the construction of molecular rotors: (1) the well-defined crystal structure enables the precise arrangement of molecular rotors within systematically designed porous structures; (2) the permanent porosity provides sufficient space for rotor rotation while also allowing guest molecules to modulate the dynamics of the molecular rotor. Hence, CPOSs show promising potential as an ideal choice for constructing molecular rotors.

In 2014, Comotti *et al.* successfully prepared the first porous molecular crystal with molecular rotors using 4,4′-bis(sulfophenylethynyl)benzene (BSPEB) and *n*-pentylamine (PA) through ionic

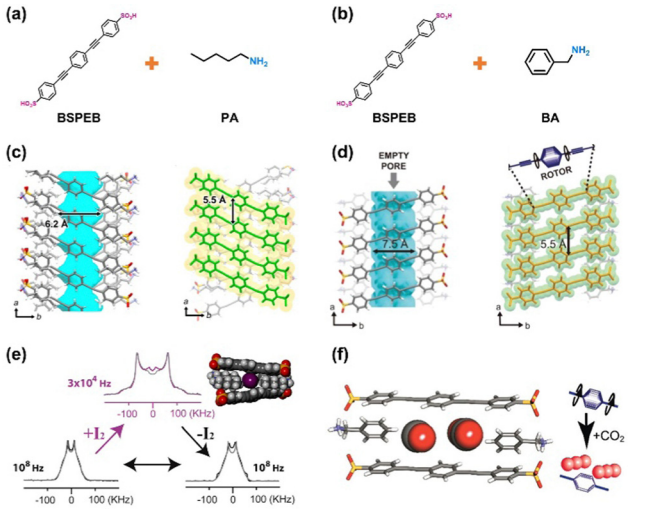

Fig. 11 (a) Chemical structure of BSPEB/PA salt. (b) Chemical structure of BSPEB/BA salt. (c) Empty channels and the distance between the two central *p*-phenylene rings in BSPEB/PA salt. Reproduced with permission.[37] Copyright 2014 American Chemical Society. (d) Empty channels and the distance between the two central *p*-phenylene rings in BSPEB/BA salt. Reproduced with permission.[38] Copyright 2017, Royal Society of Chemistry. (e) ^{2}H NMR spectra of pristine empty (left), iodine-loaded (center), and I_2-freed sample (right) (expt, black and violet lines; calc, gray lines). The exchange rates are reported. Line broadening of 8 kHz was applied to the simulated spectrum of the I_2-loaded sample. Reproduced with permission.[37] Copyright 2014 American Chemical Society. (f) Location of CO_2 molecules diffused into the channel, and schematic representation of molecular rotors in the empty and CO_2-loaded matrices. Reproduced with permission.[38] Copyright 2017, Royal Society of Chemistry.

bonding (Fig. 11(a)).[37] The adsorption capacity of CO_2, reaching 50 $cm^3\ g^{-1}$ at 195 K and 0.8 bar, serves as conclusive evidence for permanent porosity. Further analysis of the crystal structure reveals the presence of ample space, allowing for the rotation of rod-like *p*-phenylene rotors (Fig. 11(b)). Additionally, ^{2}H solid-state NMR spectroscopy elucidates that the rotors can achieve rapid rotation with frequencies as high as 10^8 Hz at room temperature. Intriguingly, the rotor dynamics could be switched off and on by I_2 absorption/desorption. Upon exposure of the crystals to I_2 vapor, a significant impeding influence is observed on the dynamics of the rotors, resulting in a drastic reduction in rotor frequency by four orders of magnitude to 3×10^4 Hz (Fig. 11(e)). This decrement can be attributed to the hindrance caused by the trapped I_2 molecules, impeding the rotation of the benzene ring. However, subsequent treatment of the porous crystals under vacuum conditions effectively eliminates the adsorbed I_2, leading to the restoration of the porous molecular crystal's pristine state with fast rotor dynamics. Subsequently, employing the same strategy, the same research group successfully utilized the organic acid BSPEB along with *n*-benzylamine (BA) in 2017 to fabricate a novel CPOS with permanent porosity and ultra-fast molecular rotors (Fig. 11(b)).[38] The *p*-phenylene rotor is elegantly positioned within the core of the rod molecule, reminiscent of a wheel gracefully affixed to an axle, and ingeniously nestled between two triple bonds, thus showcasing a virtually barrier-free rotation (Fig. 11(d)). The extremely fast rotor dynamics can be manipulated by simple exposure to

gaseous CO_2. The rotor speed can be reduced from the extremely fast regime of 10^7 Hz at 216 K to 10^5 Hz, and fully recovered after removing CO_2 molecules under vacuum (Fig. 11(f)). Therefore, incorporating molecular rotors and porosity in CPOSs is a practical approach to prepare high speed molecular rotors, and modulating the dynamics of the rotor through guest molecules has promising prospects for the application in tunable molecular devices and gas sensors.

4.8 Fluorescence modulation

Fluorescence modulation plays a significant role in various fields, such as biological imaging, optoelectronic devices, sensors, and detectors.[106] CPOSs, possessing well-defined crystalline structures, can incorporate fluorescent moieties, endowing them with fluorescence properties. Furthermore, due to their permanent porosity, different guest molecules can interact with the fluorescent moieties, enabling the modulation of fluorescence performance. Therefore, CPOSs have potential for applications in the field of fluorescence manipulation.

In 2013, Tohnai *et al.* constructed a *dia* topology CPOS (*d*-POS-1) using triphenylamine and fluorescent disulfonic acid (Fig. 12(a)).[31] *d*-POS-1 exhibits permanent porosity, as demonstrated by CO_2 sorption at 195 K (Fig. 12(b)), allowing for the retention of its open pore structure during the process of guest adsorption and desorption. *d*-POS-1 exhibits blue fluorescence with a peak at 420 nm originating in the styryl group in the host framework. It also demonstrates extensive and tunable fluorescence behaviour when adsorbing guest molecules. As shown in Fig. 12(c) and (d), the fluorescence colour shifts from blue to green upon binding with electron-donor molecules (*e.g.*, *N*,*N*-dimethylaniline and its derivatives), while fluorescence quenching occurs when interacting with electron-acceptor molecules (*e.g.* nitrobenzene). These dynamic and guest-responsive fluorescence properties provide guidance for the development of molecular sensors and memory devices.

4.9 Room-temperature phosphorescence

In recent years, room temperature phosphorescent materials have emerged as a vibrant research frontier due to their pivotal applications in organic light-emitting diodes (OLEDs) and high-resolution imaging.[107–109] The manifestation of room-temperature phosphorescence in organic materials necessitates intricate molecular engineering and precise intermolecular interactions. Essentially, the design for RTP materials revolves around two crucial factors: firstly, the facilitation of the intersystem crossing (ISC) process to achieve the triplet excited state; secondly, the effective mitigation of nonradiative transitions in the triplet state excitons.[110]

Porous organic materials have the potential to serve as exceptional host frameworks for dispersing luminescent molecules, facilitating the inhibition of energy transfer and impeding the undesired nonradiative decay processes. Consequently, CPOSs bearing permanent porosity and tailored structure exhibit promising prospects for their application in realizing RTP applications. Recently, Tohnai *et al.* ingeniously orchestrated the structural manipulation through steric hindrance to fabricate cage-like sodalite-type CPOSs (Fig. 13(a)), boasting pores larger than 20 Å and narrow windows with a maximum width of less than 8 Å.[33] The unique cage-like structure allows organic molecules to be confined within the pores, rendering CPOSs highly desirable as host frameworks for luminescent molecules. Notably, AdPS/TPMA-I with permanent porosity, possessing iodine exposed on the pore surface (Fig. 13(b)), can effectively confine pyrene molecules by simple recrystallization. Through external heavy atom effects to promote intersystem crossing from the

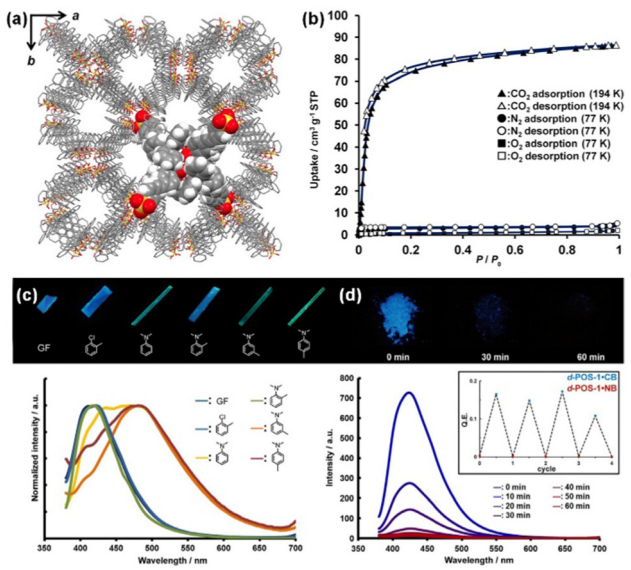

Fig. 12 (a) Crystal structure of *d*-POS-1 without guest molecules. (b) Gas adsorption isotherms on the *d*-POS-1. (c) Photographs under UV irradiation (k = 365 nm) and normalized fluorescent spectra of *d*-POS-1 without guest molecules (GF) and including *N*,*N*-dimethylaniline and its derivatives. (d) Photographs and fluorescent modulation depending on the adsorption of nitrobenzene. Reproduced with permission.[31] Copyright 2013 Elsevier.

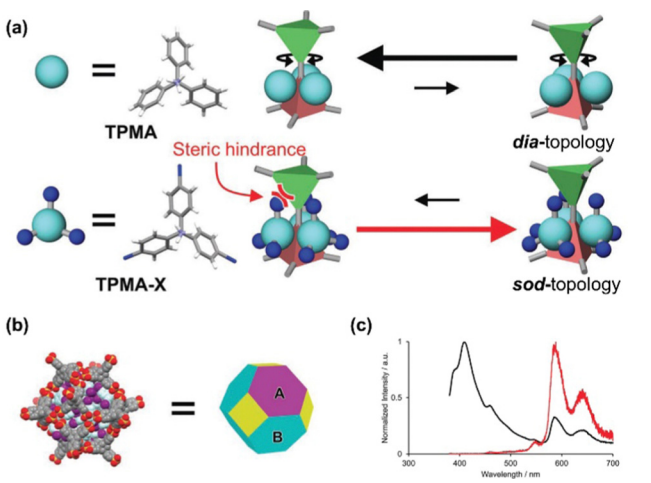

Fig. 13 (a) Strategy for the formation of different topology through steric hindrance. (b) schematic representation of the cage structure of AdPS/TPMA-I. (c) Steady-state photoluminescence spectrum (black line, excitation at 365 nm) and phosphorescence spectrum (red line, excitation at 365 nm) of pyrene⊂AdPS/TPMA-I at 298 K in the air. Reproduced with permission.[33] Copyright 2023 Wiley-VCH.

excited singlet state to the excited triplet state, suppression of thermal vibration of triplet excitons, and the prevention of quenching and increase of triplet excitons by the protection from oxygen, AdPS/TPMA-I successfully induced RTP of pyrene in air, which was further evidenced by the 550–650 nm peak in the steady-state photoluminescence spectrum belonging to the RTP of pyrene present in the cage (Fig. 13(c)). Hence, integrating luminescent molecules into CPOSs is an effective strategy to prepare organic RTP materials, which can be applied to various types of luminescent molecules to construct RTP materials with different colours.

4.10 Catalysis

Porous materials play a crucial role in the field of catalysis.[111,112] Highly developed porous structures and tunable surface properties provide a platform for catalytic reactions. First, porous materials possess large specific surface areas and abundant porous structures, offering a multitude of active sites and adsorption spaces, which facilitates the adsorption of reactants and enhances catalytic reaction activity. Second, the rational design and functionalization of porous materials can optimize the selectivity and efficiency of catalytic reactions. Moreover, porous materials exhibit excellent stability and regenerability, thus reducing catalyst loss and regeneration costs.

CPOSs, as catalysts, possess the following advantages: (1) CPOSs possess porous structures and high microporous surface areas, allowing for the adsorption of substrate molecules and providing ample reaction sites; (2) the channels contain acid/base functional groups that serve as acid/base catalytic sites for promoting reactions; (3) CPOSs exhibit excellent regenerability, allowing for the recovery of catalytic activity after a decline in performance. Therefore, CPOSs have great potential for applications in catalytic reactions.

In 2021, Belokon *et al.* utilized four different aniline derivatives and two aromatic sulfonic acids to synthesize a series of 3D CPOSs.[113] These CPOSs were employed as metal-free heterogeneous Brønsted acid catalysts, achieving highly efficient catalysis for epoxide ring-opening and acetal formation reactions. Among them, F2, derived from TSPM and TAPM, demonstrated exceptional conversion of various aldehydes to their corresponding acetals with a remarkable yield of up to 99%. Additionally, the catalyst could be easily recovered *via* filtration, and the recovered catalyst maintained its catalytic activity even after being reused for more than five cycles without a notable loss in efficiency. This study provides valuable insights for the future application of CPOSs in catalytic reactions.

5. Conclusion and perspective

5.1 Conclusion

In recent years, CPOSs, as an emerging class of crystalline porous organic materials, have achieved significant research progress, highlighting their immense potential for development. Currently, stable CPOSs with permanent porosity can be synthesized through various strategies involving the modulation of tecton types, acidity/basicity, and topology. Compared with other porous organic materials, CPOSs are constructed using ionic bonds, providing them with distinct characteristics. Additionally, CPOSs exhibit permanent porosity and polar nano-confined channels, showcasing potential applications in proton conduction, rapid guest molecule transport, NLC, AWH, catalysis, fluorescence modulation, and various other fields. However, this emerging field of CPOSs is still in a stage of rapid development, presenting both challenges and opportunities.

5.2 Perspective

5.2.1 Synthesis of novel functional CPOSs. Although the construction of CPOSs with permanent porosity can be achieved by manipulating tecton types, acidity/basicity, and topology, the number of reported CPOSs remains limited. Moreover, their surface areas are lower than other crystalline porous materials such as MOFs and COFs, which hinders the provision of a wide range of choices for different application scenarios. Therefore, developing novel organic acid/base tectons, including the rational design of acid/base groups, symmetry, and functional moieties, and exploring new preparation methods based on existing synthetic strategies, can facilitate the synthesis of functionally oriented CPOSs.

5.2.2 Precise directional synthesis of CPOSs. Ionic bonds are flexible and non-directional, making it challenging to predict the precise structure of CPOSs using reticular chemistry, as in the case of COF materials. Recently, Coric *et al.* demonstrated a novel approach by selectively modifying specific groups around ions and placing them in a spatially shielded nonpolar hydrocarbon environment, exposing charged moieties in only one direction.[114] By introducing steric hindrance, they facilitated the directed approach of oppositely charged ions, resulting in ionic bonds with a certain degree of directionality. These types of ionic bonds can connect molecular fragments with linear geometry over distances of up to 2 nm. Thus, utilizing directional ionic bonds seems to be an effective approach for the precise construction of CPOSs.

5.2.3 Artificial intelligence-assisted synthesis of CPOSs. Artificial intelligence (AI) is a burgeoning field that has emerged recently. It primarily focuses on studying and developing theories, methods, technologies, and applications to simulate and achieve human intelligence. The goal of AI is to enable computers to learn, reason, think, and make decisions in ways similar to humans, thereby solving complex problems and performing various tasks. Currently, numerous researchers in the field of chemistry and materials have devoted themselves to this area, utilizing techniques such as machine learning to predict the structures and properties of materials, leading to rapid advancements in the field. Recently, AI has been successfully applied in the development of MOF materials. Yaghi *et al.* developed a ChatGPT-based chemistry assistant for text mining and the prediction of MOF synthesis,[115] providing inspiration for the application of AI in the design and synthesis of other materials. Consequently, the rise of AI technology also has the potential for structural prediction and performance screening of CPOSs. By employing machine learning to study the existing structures of CPOSs, establishing a database for CPOSs, exploring and analyzing the bonding characteristics of CPOSs, and constructing neural networks specific to CPOSs, it is possible to achieve

structural prediction of CPOSs. The integration of AI is expected to further accelerate the rapid development of CPOSs.

5.2.4 Regenerability of CPOSs. To address global energy shortages and environmental pollution, people have increased the demand for the sustainability and environmental friendliness of materials. HOFs formed by hydrogen bonds exhibit excellent regenerability, but their stability is unsatisfactory. On the other hand, COFs consisting of covalent bonds offer good stability but possess poor regenerability. In contrast, the bonding energy of ionic bonds falls between covalent and hydrogen bonds, allowing CPOSs to exist stably under certain conditions while also being capable of controlled disruption and reassembly. This unique combination provides CPOSs with the stability of COFs and the regenerability of HOFs, facilitating convenient material regeneration and recycling. The remarkable regenerative abilities of CPOSs can extend the lifespan of materials and reduce dependence on finite resources. Furthermore, the regenerative nature of CPOSs can contribute to lowering production costs and provide broader development prospects for the sustainable advancement of materials.

5.2.5 "Superfluid" in CPOSs. Superfluidity, a macroscopic quantum effect, was first discovered in 1938.[116,117] For instance, ^{4}He exhibits zero viscosity and collective motion with no kinetic energy loss at a temperature of 2.17 K, demonstrating super-low resistance.[118] Similar "superfluid" phenomena exist in nanochannels within biological systems. For example, water channel proteins (aquaporins)[119] and KcsA proteins[120] in cell membranes possess nanoscale confinement channels that enable the rapid and selective transport of water molecules and potassium ions, with transport rates reaching 10^8 ions per s and 10^9 molecules per s, respectively. Combined with the inherent features of CPOSs, it has been discovered that CPOSs demonstrate fast transport phenomena for gas molecules such as CO_2, liquid molecules such as H_2O, and ions such as K^+. Hence, by systematically designing the structure of CPOSs and constructing artificial bio-inspired sub-nanometer confined channels, it is expected that the rapid transport of a wide range of molecules/ions can be achieved while providing new insights into understanding the "superfluid" phenomena in living organisms and innovation in related fields.

Currently, research in the field of CPOSs is rapidly advancing, and a plethora of novel CPOSs will emerge and find widespread applications in various fields. This burgeoning field is filled with both opportunities and challenges. We hope this new and captivating realm will attract more researchers to engage in this area, inspiring further exploration and innovation, and propelling the field toward greater development.

List of abbreviations

CPOSs	Crystalline porous organic salts
HOFs	Hydrogen-bonded organic frameworks
HCPs	Hypercrosslinked polymers
CMPs	Conjugated microporous polymers
PIMs	Polymers of intrinsic microporosity
PAFs	Porous aromatic frameworks
COFs	Covalent organic frameworks
POCs	Porous organic cages
BDS	4,4′-Biphenyldisulfonic acid
NDS	1,5-Napthalenedisulfonic acid
BPDS	4,4′-Biphenylenedisulfonic acid
SBDS	*trans*-Stilbene-4,4′-disulfonic acid
BSPEB	4,4′-Bis(sulfophenylethynyl)benzene
TCPM	Tetrakis(4-carboxylphenyl)methane
TSPM	Tetrakis(4-sulfophenyl)methane
AdPS	4,4′,4″,4‴-[Adamantane-1,3,5,7-tetrayl]tetrabenzenesulfonic acid
MTBPS	4′,4‴,4⁗,4⁗′-Methanetetrayltetrakis((1,1′-biphenyl)-4-sulfonic acid)
PA	*n*-Pentylamine
BA	*n*-Benzylamine
TPMA	Triphenylmethylamine
DAB	1,4-Diamidiniumbenzene
DACH	*trans*-1,4-Diaminocyclohexane
PDA	*p*-Phenylenediamine
DABP	4,4′-Diaminobiphenyl
TAPM	Tetrakis(4-aminophenyl)methane
TAmPM	Tetrakis(4-amidinophenyl)methane
MeOH	Methanol
THF	Tetrahydrofuran
GAA	Glacial acetic acid
1,2,4-TCB	1,2,4-Trichlorobenzene
DMF	*N*,*N*-Dimethylformamide
DMAc	*N*,*N*-Dimethylacetamide
SAPT	Symmetry-adapted perturbation theory
DA	Dubinin–Astakhov
BET	Brunauer–Emmett–Teller
NLC	Negative linear compression
PEMFCs	Proton exchange membrane fuel cell
HTS	High-throughput screening
AWH	Atmospheric water harvesting
RTP	Room-temperature phosphorescence
ISC	Intersystem crossing
OLEDs	Organic light-emitting diodes
AI	Artificial intelligence

Author contributions

G. X. and T. B. conceived the idea and led the project. D. P. conducted the theoretical calculation. G. X., D. P., and T. B. interpreted the results and wrote the manuscript.

Conflicts of interest

The authors declare no competing interests.

Acknowledgements

This study was supported by the National Key R&D program of China (2021YFA1200400), the National Natural Science

Foundation of China (no. 91956108, 22001191), and the Natural Science Foundation of Zhejiang Province (no. LZ22B010001).

Notes and references

1 B.-L. Su, C. Sanchez and X.-Y. Yang, *Hierarchically Structured Porous Materials*, Wiley-VCH Verlag & Co. KGaA, Germany, Weinheim, 2012.
2 Y. Yang, X. Song, X. Li, Z. Chen, C. Zhou, Q. Zhou and Y. Chen, *Adv. Mater.*, 2018, **30**, 1706539.
3 S. Das, P. Heasman, T. Ben and S. Qiu, *Chem. Rev.*, 2017, **117**, 1515–1563.
4 X.-Y. Yang, L.-H. Chen, Y. Li, J. Claire Rooke, C. Sanchezc and B.-L. Su, *Chem. Soc. Rev.*, 2017, **46**, 481–558.
5 S. Xu, Y. Luo and B. Tan, *Macromol. Rapid Commun.*, 2013, **34**, 471–484.
6 N. Fontanals, R. M. Marcé, F. Borrull and P. A. G. Cormack, *Polym. Chem.*, 2015, **6**, 7231–7244.
7 L. Tan and B. Tan, *Chem. Soc. Rev.*, 2017, **46**, 3322–3356.
8 J. X. Jiang, F. Su, A. Trewin, C. D. Wood, N. L. Campbell, H. Niu, C. Dickison, A. Y. Ganin, M. J. Rosseinsky, Y. Z. Khimyak and A. I. Cooper, *Angew. Chem., Int. Ed.*, 2007, **46**, 8574–8578.
9 Y. Xu, S. Jin, H. Xu, A. Nagai and D. Jiang, *Chem. Soc. Rev.*, 2013, **42**, 8012–8031.
10 L. Chen, Y. Honsho, S. Seki and D. Jiang, *J. Am. Chem. Soc.*, 2010, **132**, 6742–6748.
11 P. M. Budd, B. S. Ghanem, S. Makhseed, N. B. Mckeown, K. J. Msayib and C. E. Tattershall, *Chem. Commun.*, 2004, 230–231.
12 N. B. McKeown, P. M. Budd, K. J. Msayib, B. S. Ghanem, H. J. Kingston, C. E. Tattershall, S. Makhseed, K. J. Reynolds and D. Fritsch, *Chem. – Eur. J.*, 2005, **11**, 2610–2620.
13 N. B. McKeown and P. M. Budd, *Chem. Soc. Rev.*, 2006, **35**, 675–683.
14 T. Ben, H. Ren, S. Ma, D. Cao, J. Lan, X. Jing, W. Wang, J. Xu, F. Deng, J. M. Simmons, S. Qiu and G. Zhu, *Angew. Chem., Int. Ed.*, 2009, **48**, 9457–9460.
15 T. Ben, C. Pei, D. Zhang, J. Xu, F. Deng, X. Jing and S. Qiu, *Energy Environ. Sci.*, 2011, **4**, 3991–3999.
16 T. Ben and S. Qiu, *CrystEngComm*, 2013, **15**, 17–26.
17 C. S. Diercks and O. M. Yaghi, *Science*, 2017, **355**, eaal1585.
18 X. Feng, X. Ding and D. Jiang, *Chem. Soc. Rev.*, 2012, **41**, 6010–6022.
19 S. Y. Ding and W. Wang, *Chem. Soc. Rev.*, 2013, **42**, 548–568.
20 L. Chen, P. S. Reiss, S. Y. Chong, D. Holden, K. E. Jelfs, T. Hasell, M. A. Little, A. Kewley, M. E. Briggs, A. Stephenson, K. Mark Thomas, J. A. Armstrong, J. Bell, J. Busto, R. Noel, J. Liu, D. M. Strachan, P. K. Thallapally and A. I. Cooper, *Nat. Mater.*, 2014, **13**, 954–960.
21 T. Hasell and A. I. Cooper, *Nat. Rev. Mater.*, 2016, **1**, 16053.
22 X. Yang, Z. Ullah, J. Fraser Stoddart and C. T. Yavuz, *Chem. Rev.*, 2023, **123**, 4602–4634.
23 R.-B. Lin, Y. He, P. Li, H. Wang, W. Zhou and B. Chen, *Chem. Soc. Rev.*, 2019, **48**, 1362–1389.
24 Z. Zhang, Y. Ye, S. Xiang and B. Chen, *Acc. Chem. Res.*, 2022, **55**, 3752–3766.
25 Z. Fan, Y. Zou, C. Liu, S. Xiang and Z. Zhang, *Chem. – Eur. J.*, 2022, **28**, e202200422.
26 G. Xing, T. Yan, S. Das, T. Ben and S. Qiu, *Angew. Chem., Int. Ed.*, 2018, **57**, 5345–5349.
27 G. Xing, I. Bassanetti, S. Bracco, M. Negroni, C. Bezuidenhout, T. Ben, P. Sozzani and A. Comotti, *Chem. Sci.*, 2019, **10**, 730–736.
28 Y. Zhao, C. Fan, C. Pei, X. Geng, G. Xing, T. Ben and S. Qiu, *J. Am. Chem. Soc.*, 2020, **142**, 3593–3599.
29 S. Yu, G.-L. Xing, L.-H. Chen, T. Ben and B.-L. Su, *Adv. Mater.*, 2020, **32**, 2003270.
30 S. Zhang, J. Fu, S. Das, K. Ye, W. Zhu and T. Ben, *Angew. Chem., Int. Ed.*, 2022, **61**, e202208660.
31 A. Yamamoto, T. Hirukawa, I. Hisaki, M. Miyata and N. Tohnai, *Tetrahedron Lett.*, 2013, **54**, 1268–1273.
32 T. Ami, K. Oka, K. Tsuchiya and N. Tohnai, *Angew. Chem., Int. Ed.*, 2022, **61**, e202202597.
33 H. Sei, K. Oka, H. Sotome, H. Miyasaka and N. Tohnai, *Small*, 2023, 2301887.
34 I. Brekalo, D. E. Deliz, L. J. Barbour, M. D. Ward, T. Friščić and K. Travis Holman, *Angew. Chem., Int. Ed.*, 2020, **59**, 1997–2002.
35 M. O'Shaughnessy, A. C. Padgham, R. Clowes, M. A. Little, M. C. Brand, H. Qu, A. G. Slater and A. I. Cooper, *Chem. – Eur. J.*, 2023, **29**, e202302420.
36 A. Karmakar, R. Illathvalappil, B. Anothumakkool, A. Sen, P. Samanta, A. V. Desai, S. Kurungot and S. K. Ghosh, *Angew. Chem., Int. Ed.*, 2016, **55**, 10667–10671.
37 A. Comotti, S. Bracco, A. Yamamoto, M. Beretta, T. Hirukawa, N. Tohnai, M. Miyata and P. Sozzani, *J. Am. Chem. Soc.*, 2014, **136**, 618–621.
38 S. Bracco, T. Miyano, M. Negroni, I. Bassanetti, L. Marchio', P. Sozzani, N. Tohnai and A. Comotti, *Chem. Commun.*, 2017, **53**, 7776–7779.
39 A. P. Côté, A. I. Benin, N. W. Ockwig, M. O'Keeffe, A. J. Matzger and O. M. Yaghi, *Science*, 2005, **310**, 1166–1170.
40 D. Jiang, *Chem*, 2020, **6**, 2461–2483.
41 G. Xing, W. Zheng, L. Gao, T. Zhang, X. Wu, S. Fu, X. Song, Z. Zhao, S. Osella, M. Martínez-Abadía, H. I. Wang, J. Cai, A. Mateo-Alonso and L. Chen, *J. Am. Chem. Soc.*, 2022, **144**, 5042–5050.
42 T. Tozawa, J. T. A. Jones, S. I. Swamy, S. Jiang, D. J. Adams, S. Shakespeare, R. Clowes, D. Bradshaw, T. Hasell, S. Y. Chong, C. Tang, S. Thompson, J. Parker, A. Trewin, J. Bacsa, A. M. Slawin, A. Steiner and A. I. Cooper, *Nat. Mater.*, 2009, **8**, 973–978.
43 L. Zhang, L. Xiang, C. Hang, W. Liu, W. Huang and Y. Pan, *Angew. Chem., Int. Ed.*, 2017, **56**, 7787–7791.
44 K. Su, W. Wang, S. Du, C. Ji and D. Yuan, *Nat. Commun.*, 2021, **12**, 3703.
45 Y. He, S. Xiang and B. Chen, *J. Am. Chem. Soc.*, 2011, **133**, 14570–14573.
46 A. Corma, *Chem. Rev.*, 1997, **97**, 2373–2420.
47 X. Bu, P. Feng and G. D. Stucky, *Science*, 1997, **278**, 2080–2085.
48 W. Vermeiren and J.-P. Gilson, *Top. Catal.*, 2009, **52**, 1131–1161.

49 T. Adachi and M. D. Ward, *Acc. Chem. Res.*, 2016, **49**, 2669–2679.
50 C. C. Evans, L. Sukarto and M. D. Ward, *J. Am. Chem. Soc.*, 1999, **121**, 320–325.
51 K. T. Holman, A. M. Pivovar and M. D. Ward, *Science*, 2001, **294**, 1907–1911.
52 M. J. Horner, K. T. Holman and M. D. Ward, *J. Am. Chem. Soc.*, 2007, **129**, 14640–14660.
53 Y. Z. Liu, C. H. Hu, A. Comotti and M. D. Ward, *Science*, 2011, **333**, 436–440.
54 Y. Z. Liu, W. C. Xiao, J. J. Yi, C. H. Hu, S. J. Park and M. D. Ward, *J. Am. Chem. Soc.*, 2015, **137**, 3386–3392.
55 S. A. Boer, M. Morshedi, A. Tarzia, C. J. Doonan and N. G. White, *Chem. – Eur. J.*, 2019, **25**, 10006–10012.
56 M. Morshedi and N. G. White, *CrystEngComm*, 2017, **19**, 2367–2371.
57 M. Morshedi, M. Thomas, A. Tarzia, C. J. Doonan and N. G. White, *Chem. Sci.*, 2017, **8**, 3019–3025.
58 M. Morshedi, J. S. Ward, P. E. Kruger and N. G. White, *Dalton Trans.*, 2018, **47**, 783–790.
59 M. Thomas, T. Anglim Lagones, M. Judd, M. Morshedi, M. L. O'Mara and N. G. White, *Chem. – Asian J.*, 2017, **12**, 1587–1597.
60 N. G. White, *Dalton Trans.*, 2019, **48**, 7062–7068.
61 W. B. Liang, F. Carraro, M. B. Solomon, S. G. Bell, H. Amenitsch, C. J. Sumby, N. G. White, P. Falcaro and C. J. Doonan, *J. Am. Chem. Soc.*, 2019, **141**, 14298–14305.
62 N. Tohnai, Y. Mizobe, M. Doi, S. Sukata, T. Hinoue, T. Yuge, I. Hisaki, Y. Matsukawa and M. Miyata, *Angew. Chem., Int. Ed.*, 2007, **46**, 2220–2223.
63 A. Yamamoto, S. Uehara, T. Hamada, M. Miyata, I. Hisaki and N. Tohnai, *Cryst. Growth Des.*, 2012, **12**, 4600–4606.
64 A. Yamamoto, T. Hamada, I. Hisaki, M. Miyata and N. Tohnai, *Angew. Chem., Int. Ed.*, 2013, **52**, 1709–1712.
65 A. Yamamoto, T. Hasegawa, T. Hamada, T. Hirukawa, I. Hisaki, M. Miyata and N. Tohnai, *Chem. – Eur. J.*, 2013, **19**, 3006–3016.
66 T. Miyano, N. Okada, R. Nishida, A. Yamamoto, I. Hisaki and N. Tohnai, *Chem. – Eur. J.*, 2016, **22**, 15430–15436.
67 T. Hasegawa, K. Ohkubo, I. Hisaki, M. Miyata, N. Tohnai and S. Fukuzumi, *Chem. Commun.*, 2016, **52**, 7928–7931.
68 R. Akai, K. Oka, N. Okada, T. Ami and N. Tohnai, *Eur. J. Org. Chem.*, 2023, **26**, e202300417.
69 X. Wang, M. Simard and J. D. Wuest, *J. Am. Chem. Soc.*, 1994, **116**, 12119–12120.
70 N. Malek, T. Maris, M. È. Perron and J. D. Wuest, *Angew. Chem., Int. Ed.*, 2005, **44**, 4021–4025.
71 K. E. Maly, E. Gagnon, T. Maris and J. D. Wuest, *J. Am. Chem. Soc.*, 2007, **129**, 4306–4322.
72 M. Simard, D. Su and J. D. Wuest, *J. Am. Chem. Soc.*, 1991, **113**, 4696–4698.
73 I. Hisaki, C. Xin, K. Takahashi and T. Nakamura, *Angew. Chem., Int. Ed.*, 2019, **58**, 11160–11170.
74 P. T. Edwards, L. K. Saunders, A. R. Pallipurath, A. J. Britton, E. A. Willneff, E. J. Shotton and S. L. M. Schroeder, *Cryst. Growth Des.*, 2021, **21**, 6332–6340.
75 A. J. Cruz-Cabeza, *CrystEngComm*, 2012, **4**, 6362–6365.
76 A. Lemmerer, S. Govindraju, M. Johnston, X. Motloung and K. L. Savig, *CrystEngComm*, 2015, **17**, 3591–3595.
77 Calculated using Advanced Chemistry Development (ACD/Labs) Software V11.02 (©1994–2023 ACD/Labs).
78 D. W. Kang, M. Kang, H. Kim, J. H. Choe, D. W. Kim, J. R. Park, W. R. Lee, D. Moon and C. S. Hong, *Angew. Chem., Int. Ed.*, 2019, **58**, 16152–16155.
79 O. M. Yaghi, M. O'Keeffe, N. W. Ockwig, H. K. Chae, M. Eddaoudi and J. Kim, *Nature*, 2003, **423**, 705–714.
80 A. P. Côté, H. M. El-Kaderi, H. Furukawa, J. R. Hunt and O. M. Yaghi, *J. Am. Chem. Soc.*, 2007, **129**, 12914–12915.
81 P. Muang-Non, C. Richardson and N. G. White, *Angew. Chem., Int. Ed.*, 2023, **62**, e202212962.
82 G. Bolla and A. Nangia, *Cryst. Growth Des.*, 2012, **12**, 6250–6259.
83 W. Steele, *Chem. Rev.*, 1993, **93**, 2355–2378.
84 R. H. Baughman, S. Stafström, C. X. Cui and S. O. Dantas, *Science*, 1998, **279**, 1522–1524.
85 A. L. Goodwin, M. Calleja, M. J. Conterio, M. T. Dove, J. S. O. Evans, D. A. Keen, L. Peters and M. G. Tucker, *Science*, 2008, **319**, 794–797.
86 A. E. Aliev, J. Oh, M. E. Kozlov, A. A. Kuznetsov, S. L. Fang, A. F. Fonseca, R. Ovalle, M. D. Lima, M. H. Haque, Y. N. Gartstein, M. Zhang, A. A. Zakhidov and R. H. Baughman, *Science*, 2009, **323**, 1575–1578.
87 Y. Wang, K. S. Chen, J. Mishler, S. C. Cho and X. C. Adroher, *Appl. Energy*, 2011, **88**, 981–1007.
88 S. J. Peighambardoust, S. Rowshanzamir and M. Amjadi, *Int. J. Hydrogen Energy*, 2010, **35**, 9349–9384.
89 Y. Wang, T. Yan and T. Ben, *Chem. Res. Chin. Univ.*, 2020, **36**, 976–980.
90 T. Dudev and C. Lim, *Acc. Chem. Res.*, 2014, **47**, 3580–3587.
91 R. MacKinnon, *Angew. Chem., Int. Ed.*, 2004, **43**, 4265–4277.
92 D. A. Doyle, J. M. Cabral, R. A. Pfuetzner, A. Kuo, J. M. Gulbis, S. L. Cohen, B. T. Chait and R. MacKinnon, *Science*, 1998, **280**, 69–77.
93 S. Y. Noskov, S. Bernèche and B. Roux, *Nature*, 2004, **431**, 830–834.
94 W. Xin, J. Fu, Y. Qian, L. Fu, X. Y. Kong, T. Ben, L. Jiang and L. Wen, *Nat. Commun.*, 2022, **13**, 1701.
95 S. Zhang, J. Fu, G. Xing, W. Zhu and T. Ben, *ChemistryOpen*, 2023, **12**, e202300046.
96 W. Song, Z. Zheng, A. H. Alawadhi and O. M. Yaghi, *Nat. Water*, 2023, **1**, 626–634.
97 N. Hanikel, X. Pei, S. Chheda, H. Lyu, W. Jeong, J. Sauer, L. Gagliardi and O. M. Yaghi, *Science*, 2021, **374**, 454–459.
98 H. Kim, S. Yang, S. R. Rao, S. Narayanan, E. A. Kapustin, H. Furukawa, A. S. Umans, O. M. Yaghi and E. N. Wang, *Science*, 2017, **356**, 430–434.
99 H. L. Nguyen, N. Hanikel, S. J. Lyle, C. Zhu, D. M. Proserpio and O. M. Yaghi, *J. Am. Chem. Soc.*, 2020, **142**, 2218–2221.
100 G. Xing, S. Zhang, W. Zhu and T. Ben, *Angew. Chem., Int. Ed.*, 2023, **62**, e202215074.
101 V. A. Russell, M. C. Etter and M. D. Ward, *Chem. Mater.*, 1994, **6**, 1206–1217.

102 K. T. Holman, A. M. Pivovar, J. A. Swift and M. D. Ward, *Acc. Chem. Res.*, 2001, **34**, 107–118.
103 J. K. Gimzewski, C. Joachim, R. R. Schlittler, V. Langlais, H. Tang and I. Johannsen, *Science*, 1998, **281**, 531–533.
104 L. Kobr, K. Zhao, Y. Q. Shen, A. Comotti, S. Bracco, R. K. Shoemaker, P. Sozzani, N. A. Clark, J. C. Price, C. T. Rogers and J. Michl, *J. Am. Chem. Soc.*, 2012, **134**, 10122–10131.
105 A. Comotti, S. Bracco and P. Sozzani, *Acc. Chem. Res.*, 2016, **49**, 1701–1710.
106 J. Zhao, K. Xu, W. Yang, Z. Wang and F. Zhong, *Chem. Soc. Rev.*, 2015, **44**, 8904–8939.
107 M. A. Baldo, D. F. O'Brien, Y. You, A. Shoustikov, S. Sibley, M. E. Thompson and S. R. Forrest, *Nature*, 1998, **395**, 151–154.
108 S. Lamansky, P. Djurovich, D. Murphy, F. Abdel-Razzaq, H. E. Lee, C. Adachi, P. E. Burrows, S. R. Forrest and M. E. Thompson, *J. Am. Chem. Soc.*, 2001, **123**, 4304–4312.
109 Y. You, *Curr. Opin. Chem. Biol.*, 2013, **17**, 699–707.
110 Y.-Q. Zhu, X.-H. Wang and M.-X. Wu, *Adv. Funct. Mater.*, 2023, 2308096.
111 Y.-Z. Chen, R. Zhang, L. Jiao and H.-L. Jiang, *Coord. Chem. Rev.*, 2018, **362**, 1–23.
112 J. Liang, Z. Liang, R. Zou and Y. Zhao, *Adv. Mater.*, 2017, **29**, 1701139.
113 A. Gak, S. Kuznetsova, Y. Nelyubina, A. A. Korlyukov, H. Li, M. North, V. Zhereb, V. Riazanov, A. S. Peregudov, E. Khakina, N. Lobanov, V. N. Khrustalev and Y. N. Belokon, *Cryst. Growth Des.*, 2021, **21**, 6364–6372.
114 I. Hutskalov, A. Linden and I. Čoric, *J. Am. Chem. Soc.*, 2023, **145**, 8291–8298.
115 Z. Zheng, O. Zhang, C. Borgs, J. T. Chayes and O. M. Yaghi, *J. Am. Chem. Soc.*, 2023, **145**, 18048–18062.
116 P. Kapitza, *Nature*, 1938, **141**, 74.
117 J. F. Allen and A. D. Misener, *Nature*, 1938, **141**, 75.
118 X. Zhang, B. Song and L. Jiang, *Acc. Chem. Res.*, 2022, **55**, 1195–1204.
119 B. L. de Groot and H. Grubmüller, *Science*, 2001, **294**, 2353–2357.
120 D. A. Doyle, J. M. Cabral, R. A. Pfuetzner, A. Kuo, J. M. Gulbis, S. L. Cohen, B. T. Chait and R. MacKinnon, *Science*, 1998, **280**, 69–77.